Defective *Slc7a7* transport reduces systemic arginine availability compromising erythropoiesis and iron homeostasis

Fernando Sotillo[1*], Judith Giroud-Gerbetant[1,2*], Jorge Couso[3], Rafael Artuch[2,4,5], Antonio Zorzano[1,6,7], Aida Ormazabal[2,6,7], Mayka Sanchez[8], Günter Weiss[9], Susanna Bodoy[1,2,10#], Manuel Palacín[1,2,4#]

[1]Institute for Research in Biomedicine Barcelona (IRB Barcelona), Barcelona, Spain; [2]Centro de Investigación Biomédica en Red Enfermedades Raras (CIBERER), Barcelona, Spain; [3]Institute of Predictive and Personalized Medicine of Cancer, Badalona, Spain; [4]Department of Clinical Biochemistry, Hospital Sant Joan de Déu (HSJD), Esplugues de Llobregat, Spain; [5]Institut de Recerca Sant Joan de Déu, Esplugues de Llobregat, Spain; [6]Department of Biochemistry and Molecular Biomedicine, University of Barcelona, Barcelona, Spain; [7]Centro de Investigación Biomédica en Red Diabetes y Enfermedades Metabólicas (CIBERDEM), Spain; [8]Faculty of Medicine and Health Sciences. Universitat Internacional de Catalunya (UIC), Sant Cugat, Spain; [9]Department of Internal Medicine II (Infectious Diseases, Immunology, Rheumatology and Pneumology), Medical University of Innsbruck, Innsbruck, Austria; [10]Department of Biosciences, University of Vic - Central University of Catalonia, Vic, Spain.

[*]These authors contributed equally

Key words: y^+LAT1, arginine, iron metabolism, macrophage, red blood cell (RBC)

Correspondence: mpalacin@irbbarcelona.org (M.P.), susanna.bodoy@irbbarcelona.org (S.B.)

ABSTRACT

Slc7a7 encodes for y^+LAT1, a transporter of cationic amino acid across the basolateral membrane of epithelial cells. Mutations in *SLC7A7* gene give rise to Lysinuric Protein Intolerance (LPI), a rare autosomal recessive disease with wide variability of complications. Intriguingly, y^+LAT1 is also involved in arginine transport in non-polarized cells such as macrophages. Here we report that complete inducible *Slc7a7* ablation in mouse compromises systemic arginine availability that alters proper erythropoiesis and that dysfunctional RBC generation leads to increased erythrophagocytosis, iron overload and an altered iron metabolism by macrophages. Herein, uncovering a novel mechanism that links amino acid metabolism to erythropoiesis and iron metabolism. Mechanistically, the iron exporter ferroportin-1 expression was compromised by increased plasma hepcidin causing macrophage iron accumulation. Strikingly, lysozyme M-cell-specific knockout mice failed to reproduce the total knockout alterations, while bone marrow transplantation experiments resulted in the resolution of macrophage iron overload but could not overcome erythropoietic defect. This study establishes a new crucial link between systemic arginine availability in erythropoiesis and iron homeostasis.

Introduction

Red blood cell (RBC) generation is a tightly regulated process where RBC homeostasis is key for proper iron recycling (de Back et al., 2014). Although extensive work has been done in the field of erythropoiesis, little is known about the impact of amino acid metabolism in this complex process. The mechanisms of RBC generation spans from bone marrow (BM) erythroid differentiation mediated by $CD169^{+}$ macrophages (Chow et al., 2013), which supports erythroblastic island formation, to the end-final stage where RBC phagocytosis by red pulp macrophages (RPMs) leads to hemoglobin breakdown and ultimately iron recycling and release (Klei et al., 2017). RBC maturation requires specific components to properly coordinate this process. Disruption in hemoglobin synthesis, which comprises one-third of the RBC protein content, leads to altered erythropoiesis (Kuhn et al., 2017; Liu et al., 2013) .Yet, hemoglobin is not the only key component as iron, erythropoietin (EPO), or ferritin are also well known to play essential roles in RBC generation (Beguin, 1998; Goldfarb et al., 2021; Moritz et al., 1997). In terms of metabolic requirements, Shima *et al.* published the impact of arginine import on erythrocyte differentiation and proliferation throughout the cationic amino acid transporter 1 (CAT1), thereby indicating a crucial role not only of the iron-related components (hemoglobin, EPO, iron and ferritin) but also of metabolites such as arginine in the generation of mature RBCs (Shima et al., 2006). Macrophages also play an important role in RBC enucleation, being thus key for the last step of RBC generation (Lee et al., 2004; Popova et al., 2009; Swartz et al., 2017).

Macrophages are a cell type that participates in diverse biological processes, including host defence and wound repair (Koh and DiPietro, 2011). Nevertheless, further roles for these cells began to emerge with the identification of specific functions of tissue-

resident macrophages, such as Kupffer cells and splenic RPMs, which are mainly involved in erythrocyte phagocytosis and iron recycling (Beaumont and Delaby, 2009; Ganz, 2012; Theurl et al., 2016), alveolar macrophages (AMs), which participate in both lung development and surfactant recycling, and osteoclasts, which contribute to bone development (Hussell and Bell, 2014; Murray and Wynn, 2011). Interest in macrophages in the context of metabolic disease has gained momentum due to a number of recent findings. Macrophage polarization is well known to be tighly linked to altered cellular metabolism including iron homeostasis and glycolysis/citric acid cycle activity (Recalcati et al., 2012; Stienstra et al., 2017). In addition, changes in L-arginine metabolism have been coupled to different immune effector phenotypes of macrophages involved in autoimmunity, infection control and activation (Bronte and Zanovello, 2005; Jha et al., 2015; Weiss and Schaible, 2015).

Lysinuric Protein Intolerance (LPI, MIM 222700) is a rare autosomal recessive disease caused by mutations in *SLC7A7* gene (solute carrier family 7) which encodes for y^+LAT1 (Palacín et al., 2001; Torrents et al., 1999) , a light subunit of the heterodimeric amino acid transporter family. Y^+LAT1 mediates the exchange of cationic amino acids (CAAs) with neutral amino acids plus sodium (Palacín et al., 2005) across the basolateral membrane of epithelial cells. Mutations in y^+LAT1 results in defective transport of CAAs, leading to reduced arginine, ornithine and lysine plasma concentration while increased in urine (Ogier de Baulny et al., 2012). Consistent with the clinical manifestations of human LPI, we have previously reported that the inducible complete loss of y^+LAT1 in mice leads to hypoargininemia, which results in urea cycle disruption and hyperammonemia. Consequently leading to reduced body weight, brain edema and pulmonary alveolar proteinosis between other complications (Bodoy et al., 2019). In addition, several studies found that patients with one or several

mutations in *Slc7a7* gene have abnormal blood count, as well as microcytic anemia (Alqarajeh et al., 2020; Rajantie et al., 1980). To date, the standard treatment for LPI mainly consists on a low-protein based diet supplemented with oral citrulline (Lukkarinen et al., 2003), where citrulline is intracellularly converted to arginine in renal epithelial cells. Hence, improving the defects in urea cycle and correcting both plasma arginine and ammonia levels (Dhanakoti et al., 1990).

Notably, y^+LAT1 also mediates arginine transport in non-polarized cells, such as macrophages. Intriguingly, y^+LAT1 was shown to drive major arginine transport in human monocytes after interferon stimulation (Rotoli et al., 2020). Thus, being one of the major arginine transporters in human monocytes, AMs and monocyte-derived macrophages (Barilli et al., 2012).

Motivated by the fact that human SLC7A7 mutations give rise to immune and hematological complications, here we questioned whether amino acid transport via *Slc7a7* has important roles for erythropoiesis and/or iron homeostasis. Using total loss-of-function of y^+LAT1, recovery with citrulline, Lysozyme M-cell-specific (i.e. myeloid-specific) knockout mice and BM transplantations, we demonstrated that the systemic metabolic condition of LPI (mainly hypoargininemia and/or hyperammonemia) leads to defective erythropoiesis and altered RBCs, prompting thus increased erythrophagocytosis ultimately leading to highly iron loaded RPMs and BMMs and hyperferritinemia. Mechanistically, depletion of extracellular arginine and increased plasma amonia levels, as a result of *Slc7a7* ablation in kidney and intestine, leads to impared development of RBCs that are more phagocyted by RPMs. Iron overload is a well known hepcidin driver through the bone morphogenic protein – 6 (BMP6) (Andriopoulos et al., 2009), hence, high levels of iron triggered hepcidin expression which in turn downregulated FPN1 in *Slc7a7* macrophages, by this way

altering iron recycling. Further analyses revealed that defective erythropoiesis was absent in the myeloid-specific knockout mouse. These findings connect two previously unrelated biological processes, namely defective RBC generation and macrophage iron accumulation, and implicate the LPI metabolic derangement as a key player in the hematologic complications of the disease.

Results

Global y$^+$LAT1 ablation in adult mice results in a drastic reduction of bone marrow macrophages and red pulp macrophages.

Y$^+$LAT1 is highly expressed in epithelial cells and in some non-polarized cells such as macrophages (Pollard, 2009; Rotoli et al., 2020). To dissect the role of y$^+$LAT1 in the immune and hematological complications of LPI, we created a y$^+$LAT1 conditional allele (*Slc7a7*$^{loxp/+}$) and generated a *Slc7a7*$^{loxp/loxp/UBC\text{-}Cre+}$ inducible knockout model that expresses Cre in all the body cells in response to tamoxifen treatment. Twelve-week-old *Slc7a7*$^{loxp/loxp/UBC\text{-}Cre+}$(*Slc7a7*$^{-/-}$, after tamoxifen induction) mice and their control *Slc7a7*$^{loxp/loxp/UBC\text{-}Cre-}$ (*Slc7a7*$^{+/+}$) littermates were first treated with tamoxifen for 7 days to induce Cre expression and were further kept on low-protein diet. As a result, y$^+$LAT1 depletion led to significant reduction of spleen weight (Figure 1A). However, consistent with previous reports that citrulline administration ameliorates hypoargininemia and hyperammonemia as well as the vast majority of the defects caused by y$^+$LAT1 ablation (Bodoy et al., 2019), 10 days of citrulline supplementation also improved spleen weight (Supplementary Figure 1A). Of note, *Slc7a7* ablation led to lower levels of F4/80-positive cells in spleen and BM sections, together with a reduced number of F4/80^{hi} cd11b^{lo} cells *in vivo* (Figure 1B-C), which were also recovered by citrulline administration (Supplementary Figure 1B-C). Besides,

circulating monocytes levels were also decreased in y$^+$LAT1-deficient mice, thereby indicating a loss of macrophage precursors (Figure 1D).

We then asked whether the decreased number of RPMs was associated with a reduced proliferation or increased apoptosis. To this end, we assessed Ki67 and caspase-3 expression in spleen sections. Indeed, Ki67 was reduced in the red pulp area of *Slc7a7*$^{-/-}$ mice, where RPMs reside (Figure 1E). Moreover, *Slc7a7*$^{-/-}$ RPMs expressed higher levels of active caspase-3 compared with those of control mice (Figure 1F). Taken together, our data suggests that y$^+$LAT1 participates in the homeostasis of BMMs and RPMs, which might be caused by both increased apoptosis and decreased levels of proliferation.

y$^+$LAT1 deficiency in myeloid cell line does not reproduce conditional knockout mice deficiencies.

We then asked whether the lack of *Slc7a7* expression in macrophages was key for the defects previously observed (Figure 1 A,C). For that purpose, we generated a myeloid cell-specific knockout mouse (*Slc7a7*$^{loxp/lox\ LysM\text{-}Cre+}$; *Slc7a7*$^{LysM-/-}$) in which Cre expression is specifically restricted to the myeloid cell lineage. Likewise, the inducible knockout mice, *Slc7a7*^{LysM}, showed a reduced expression of *Slc7a7* in RPMs, AMs and BMDMs (Supp Figure 2A-B). Nevertheless, contrary to the inducible model *Slc7a7*$^{-/-}$ (Bodoy et al., 2019), *Slc7a7*^{LysM} mice did not present reduction of y$^+$LAT1 expression in kidney, hypoargininemia or urea cycle dysfunction (e.g., increased orotic acid in urine), nor did they show a reduction in spleen size or body weight or a decrease in RPMs and BMMs numbers *in vivo* (Supp Figure 2B-G). These findings rule out the possibility that the defect comes from the lack of y$^+$LAT1 expression in the myeloid cell line and embraces the possibility that systemic reduction of arginine along

with other unbalanced amino acids and metabolites (LPI systemic metabolic condition) might underlie the observed decrease in macrophage generation and survival in total knockout mice.

Slc7a7$^{-/-}$ but not _Slc7a7_^{LysM} red pulp macrophages, have a dysfunctional iron metabolism.

Since one of the main functions of RPMs is to regulate erythrocyte degradation and iron delivery for erythropoiesis (Kohyama et al., 2009), we next focused on whether iron metabolism was compromised in both mouse models. *Slc7a7*$^{-/-}$ mice showed a dramatic iron accumulation in the BM and spleen. In contrast, abnormal iron accumulation was not visible in *Slc7a7*^{LysM} animals (Figure 2A), thus, further confirming the premise that y$^+$LAT1 deficiency in the myeloid cell line does not cause macrophage dysfunction. Citrulline treatment improved iron accumulation in the spleen and BM in *Slc7a7*$^{-/-}$ mouse (Figure 2A). In line with this finding, iron content in the liver and spleen tissue were higher in the *Slc7a7*$^{-/-}$ mice compared to its control littermates and were rescued by citrulline supplementation (Figure 2B).

We next addressed whether iron accumulation in tissues would also be reflected into higher serum ferritin levels (Cohen et al., 2010), a trait usually reported in LPI patients (Ogier de Baulny et al., 2012). Hyperferritinemia was found in the *Slc7a7* knockout mice (Figure 2C), and, as expected, the impairment was reversed by citrulline administration and no differences were observed in the *Slc7a7*^{LysM} mouse model (Figure 2C). To study whether hyperferritinemia was associated with increased inflammation (Kawasumi et al., 2014; Rosário et al., 2013), we examined IL6 plasma levels. Strikingly, control and *Slc7a7*$^{-/-}$ mice showed similar levels of IL6 (Supp Figure 3A), excluding thereby systemic inflammation as a plausible cause of increased

ferritinemia or macrophage iron retention (Theurl et al., 2016). Given that y^+LAT1 deletion resulted in a significant reduction in the number of RPMs and BMMs, we tested whether the observed iron accumulation was directly linked to macrophages. Of note, within the spleen, iron accumulation was specifically located in the resident RPMs (Figure 2D).

As a whole, these results indicate that the systemic metabolic conditions of LPI cause detrimental effects on RPM homeostasis but *Slc7a7* expression in macrophages is not required for the iron accumulation in tissue.

Slc7a7$^{-/-}$ mouse model show reduced expression of FPN1 in macrophages

To gain insight into how iron is accumulated in macrophages, we analyzed the expression of FPN1, the only known iron exporter, and its relationship to circulating concentrations of hepcidin, the major iron-regulatory hormone that interacts directly with FPN1 triggering its degradation (Nemeth et al., 2004). Of note, hepcidin plasma levels were increased in *Slc7a7*$^{-/-}$ mice (Figure 3A) which were paralleled by increased expression levels of liver hepcidin (*Hamp1*) in *Slc7a7*$^{-/-}$ mice as compared to control littermates (Figure 3B). Hepcidin levels can be regulated at the transcriptional levels by several factors such as inflammation and hepatocyte iron deposits(Sebastiani et al., 2016) . In this regard, microarray data on sorted RPMs from *Slc7a7*$^{+/+}$ and *Slc7a7*$^{-/-}$ mouse showed decreased expression of inflammatory-related pathways. Moreover, as indicated above, plasma interleukin 6 levels showed similar levels between both genotypes, thus ruling out the possibility of inflammation as a plausible cause for increased hepcidin levels (Supplementary Figure 3A-B). Nevertheless, enhanced Pearl's Prussian blue staining revealed that *Slc7a7*$^{-/-}$ liver sections showed specific localization of iron deposits in hepatocytes (Figure 3C), suggesting thus iron

accumulation as the main cause for increased hepcidin levels. The increased number of iron deposits was accompanied by a significant increase of the BMP6 (Figure 3D), a protein known to interact with hemojuvelin to further (Core et al., 2014), trigger *Hamp1* transcription and expression (Andriopoulos et al., 2009; JL et al., 2006). Thus, further supporting the premise that hepatocyte liver accumulation triggers increased hepcidin plasma levels.

Flow cytometry analysis revealed a decreased number of FPN1-positive RPMs in *Slc7a7*$^{-/-}$ compared to wildtype mice (Figure 3E). Moreover, decreased FPN1 expression in RPMs was also confirmed by western blot, where *Slc7a7*$^{-/-}$ mice show reduced levels of FPN1 in total spleen (Figure 3F).

Together, our results indicate that *Slc7a7* expression is necessary to maintain proper FPN1 expression and that its imbalance leads to an aberrant iron retention in resident macrophages.

Slc7a7$^{-/-}$ mice show exacerbated erythrophagocytosis

Our findings that *Slc7a7*$^{-/-}$ RPM were loaded with iron together with the imbalance on iron metabolism suggests that RPM function is impared in *Slc7a7*$^{-/-}$ knockout mouse. In that sense,gene expression analysis of sorted RPMs from *Slc7a7*$^{+/+}$ and *Slc7a7*$^{-/-}$ animals revealed altered expression of key RPM-associated genes (Figure 4A) (Haldar et al., 2014; Kohyama et al., 2009) further supporting an impaired RPM functioning and disrupted iron handling. Moreover, RPMs are a highly specialized erythrophagocytic cell type in which several genes have been proposed as master regulators of iron homeostasis and RBC clearance (Kohyama et al., 2009). In this regard, these animals showed increased expression of *SpiC*, the master regulator of RPM differentiation, *Msr1*, the macrophage scavenger receptor 1, and the hemoglobin

scavenger receptor *CD163* in *Slc7a7*$^{-/-}$ mice, while *Il1b* gene expression, a proinflammatory cytokine linked to erythrophagocytosis (A-Gonzalez et al., 2017; Guo et al., 2019; Kohyama et al., 2009; Oexle et al., 2003), was significantly reduced (Figure 4B) (Moestrup and Møller, 2004). This expression pattern suggested an increased erythrophagocytosis activity in *Slc7a7*$^{-/-}$ mice. To examine this effect in further detail, we measured the ertyrhophagocytosis ratio of BMDMs from wildtype and knockout mouse. Strikingly, when *Slc7a7*$^{-/-}$ and control RBCs were co-incubated with BMDMs from *Slc7a7*$^{-/-}$ or control mice, *Slc7a7*$^{-/-}$ erythrocytes were preferentially engulfed by both macrophages (Figure 4C). Hence, *ex vivo* experiments confirmed a significantly higher phagocytosis rate of RBCs derived from *Slc7a7*$^{-/-}$ deficient mice compared to RBCs from control animals. In addition, RBCs from *Slc7a7*$^{-/-}$ and control animals treated with citrulline were equally engulfed by both macrophages, demonstrating again the rescuing effect of citrulline (data not shown). These results indicate that the observed iron accumulation in macrophages is due to a defect on the RBCs rather than an alteration on the RPMs functioning.

y^{+}LAT1 depletion results in defective erythropoiesis

To understand the mechanisms underlying the defect in erythrocytes that results in increased erythrophagocytosis (Figure 4B), we performed a hematological analysis of *Slc7a7*$^{-/-}$ animals and its control littermates. *Slc7a7*$^{-/-}$ erythrocytes had a reduced mean corpuscular volume (MCV) and hemoglobin (MCH) as well as a decreased mean platelet volume (MPV), while no differences were found in *Slc7a7*^{LysM} mice (Figure 5A-F). Interestingly, erythropoietic progenitors analyzed by flow cytometry showed that *Slc7a7*$^{-/-}$ mice have a severe reduction in erythrocyte precursors (Figure 5G). The dramatic decrease in erythroid precursors implies that LPI systemic metabolic

condition caused by global *Slc7a7* ablation compromises RBC generation. In fact, erythroid precursors of *Slc7a7*^{LysM} mice were not affected (Figure 5G).

EPO is a secreted hormone responsible for stimulating RBC production and survival. Specifically, EPO has been described to stimulate RBC generation at the proerythroblast stage (Hattangadi et al., 2011). We therefore measured EPO plasma levels and found that, indeed, EPO levels were significantly decreased in *Slc7a7*$^{-/-}$ mice (Figure 5H). As a whole, these results indicate that y$^+$LAT1 plays a specific role in erythroid development at multiple proerythroblast stages, possibly orchestrated by the metabolic defects caused by *Slc7a7* ablation.

Bone marrow transplant improves iron accumulation but not the metabolic complications and erythropoietic defects

Since immature erythroid precursors were dramatically reduced in *Slc7a7*$^{-/-}$ mice (Figure 5G), RBCs had an altered MCV and MCH (Figure 5D-E), and *Slc7a7*^{LysM} animals did not show any erythropoietic defects (Figure 5A-G), we speculated that the observed alterations in the *Slc7a7*$^{-/-}$ background could be due to the modified systemic microenvironment rather than a cell-autonomous defect in the BM. For this purpose, BM cells isolated from *Slc7a7*$^{+/+}$ mice (CD45.1) were harvested and transplanted into lethally irradiated *Slc7a7*$^{-/-}$ mice (CD45.2); conversely, BM cells isolated from *Slc7a7*$^{-/-}$ mice (CD45.2) were harvested and transplanted into lethally irradiated *Slc7a7*$^{+/+}$ mice (CD45.1). Five weeks after transplantation, mice were placed on a tamoxifen diet for 7 days and then further fed a low-protein diet for 10 days prior to the sacrifice day (Figure 6A). In this setting, BM transplantation did not improve the body and spleen weight of the *Slc7a7*$^{-/-}$ animals (CD45.2) transplanted with *Slc7a7*$^{+/+}$ BM (CD45.1) (Figure 6B-C). Analysis of peripheral blood revealed that arginine plasma levels were

diminished and orotic acid levels in urine were high as a consequence of the urea cycle dysfunction (Figure 6D-E). Thus, as expected, BM transplant did not affect the main metabolic complications of LPI. Interestingly, *Slc7a7*$^{-/-}$ mice receiving *Slc7a7*$^{+/+}$ BM, did not present iron accumulation in the spleen nor differences in the MCH (Figure 6F, J) and exhibited a tendency towards lower plasma ferritin levels (Figure 6G). This finding thus indicates that BM transplant can specifically rescue iron metabolism defects. Conversely, *Slc7a7*$^{-/-}$ transplanted mice exhibited a vast decrease in erythroid progenitors I-IV compartments together with reduced MCV (Figure 6H), reaffirming the profound systemic effect of y$^+$LAT1 deficiency on RBC generation and homeostasis.

Discussion

The y$^+$LAT1 transporter is a cationic/neutral amino acid exchanger that provides arginine for different processes in the organism. Proper arginine availability is essential for a normal urea cycle (Morris, 2002). The defiency of y$^+$LAT1 transporter in LPI condition, causes systemic hypoargininemia, which due to the shortage of urea cycle intermediates, results in hyperammonemia (Bodoy et al., 2019). In our mouse model of LPI, as shown here, this metabolic derrangement causes erythropoiesis failure, whereas y$^+$LAT1 expression in macrophages is not enough to cause impared development of RBCs in the *Slc7a7*^{LysM} mouse model. In this regard, little is known about the role of amino acid availability in erythropoiesis. The impact of L-arginine in erythrocytes is highlighted by the fact that ablation of the arginine transporter CAT1 in mouse results in perinatal death and anemia (Perkins et al., 1997) and that L-arginine-mediated CAT1 transport participates in erythrocyte differentiation and proliferation *in* vitro (Shima et al., 2006). Moreover, the L-arginine catalytic enzyme endothelial nitric

oxide synthase (eNOS) can be found in erythrocytes, where parasite-arginine deprivation decreases deformability of these cells as a result of reduced NO production (Cobbold et al., 2016). Here we show that upon ablation of *Slc7a7* in all cells, erythrocytes present reduced mean corpuscular volume and mean corpuscular hemoglobine, which has also been also described in LPI patients (Al-Qattan et al., 2021). Since arginine is the metabolite recovered by citrulline administration, we hypothesized that hypoargininemia plays a key role in erythropoiesis and RBC size.

Altered RBCs in *Slc7a7*$^{-/-}$ leads to increased erythrophagocitosis. Furthermore, bone marrow-derived macrophages from y^{+}LAT1 knock out mice did not show an increased rate of erythrophagocytosis when exposed to control erythrocytes, further supporting that the observed abnormalities in *Slc7a7*$^{-/-}$ RPMs (i.e. increased markers of erythrophagocytosis) are primed by altered erythrocytes rather than by a cell-autonomous defect of RPMs.

RPMs prime erythrocyte degradation and iron recycling, and defects in numerous pathways can lead to iron overload in macrophages (Knutson et al., 2005). Such pathological conditions can thus lead to compromised iron metabolism and have an impact on macrophages (Ganz, 2012; Soares and Hamza, 2016). For instance, aged or damaged erythrocytes can express “eat me” signals and acutely trigger the erythrophagocytosis machinery (Luo et al., 2016; Oldenborg, 2000; Park and Kim, 2017) subsequently causing iron accumulation in RPMs (Dichtl et al., 2018) as we clearly observed in the *Slc7a7*$^{-/-}$ model. We postulate therefore that defective arginine availability is also at the basis of iron accumulation because citrulline administration recovers normal iron levels in liver, spleen and BM, and they are also not present in *Slc7a7*^{LysM} tissues.

FPN1 is the only known iron exporter involved in iron efflux in macrophages. Mechanistically, FPN1 is regulated at the protein level by hepcidin, which mediates its degradation (Drakesmith et al., 2015). In this regard, the increased hepatic iron content and ferritin levels (Nemeth and Ganz, 2009) would be at the root of induced hepcidin expression as depicted by increased *BMP6* liver mRNA expression. As a consequence of increased plasma hepcidin, *Slc7a7*$^{-/-}$ show decreased FPN1 expression in RPMs, which was further confirmed by both flow cytometry and western blot analysis. Presumably, in this LPI mouse model the dysfunctional RBC generation increases erythrophagocytosis by a mechanism that, at the same time, leads to overwork of the fewer RPMs and disrupted iron handling by altered FPN1 homeostasis.

Erythroblast differentiation is orchestrated mainly by EPO expression (Jelkmann, 2011; Moritz et al., 1997). Our findings that *Slc7a7*$^{-/-}$ mice show reduced EPO in circulation, highlights the importance of *Slc7a7*-mediated systemic arginine availability. However, while BM transplant failed to rescue the hematological alterations, it did recover macrophage iron accumulation, suggesting thus two additive mechanisms. On one hand defects in RBC maturation are caused by an unbalanced systemic metabolic environment rather than by a cell-autonomous defect. On the other hand, macrophage iron accumulation also requires *Slc7a7* ablation in macrophages. Future work is needed to elucidate the link between *Slc7a7*-mediated systemic arginine availability and EPO production, and between macrophage y^+LAT1 and FPN1 expression.

Substantial advances in the research field of LPI have been scarce during the last decade, which can be probably explained by the huge phenotypic variability found among LPI patients (Al-Qattan et al., 2021; Ogier de Baulny et al., 2012; Posey et al.,

2014). In a previous work we showed that the inducible total *Slc7a7*$^{-/-}$ mouse model recapitulates the main hallmarks of the human LPI complications, such as hypoargininemia, hyperammonemia and PAP (Bodoy et al., 2019; Ogier de Baulny et al., 2012; Parto et al., 1994). In the current work we show that *Slc7a7*$^{-/-}$ mouse model has increased erytrophagocitosis, elevated serum ferritin, altered hemogram and abnormal iron retention in macrophages (Ogier de Baulny et al., 2012). Moreover, the systemic metabolic condition of LPI is an essential driver for the hematologic complications. In addition, *Slc7a7*$^{-/-}$ mice showed deficient erythropoyesis, a trait that paralels the reduced number of reticulocytes in some LPI patients, an alteration that has not been fully explored (Al-Qattan et al., 2021). Our results shifted the spotlight of increased erythrophagocytosis by abnormally functioning macrophages to altered erythrocytes.

Historically, systemic metabolic condition and immune-hematologic complications of LPI have been considered as independent entities, such is the case that some authors concerned about a potential detrimental effect of citrulline treatment in the development of immune complications (Ogier de Baulny et al., 2012). Nevertheless, more recently low argininemia was revealed as a poor prognosis factor in LPI (Mauhin et al., 2017). Now, our work upholds the premise that the handling of the metabolic derangements could prove beneficial not only for the metabolic hallmarks of the diseases but also for the reported hematologic complications of the patients.

Author Contributions

F.S., J.G., and S.B. designed and performed experiments, interpreted and analyzed data. J.G., S.B., and M.P. designed research and wrote the manuscript with input from

405 all of the authors. J.C. performed research. G.W and M.S. provided reagents and
406 provided intellectual input. A.O., R.A. and A.Z. provided reagents.
407 The authors declare no competing financial interests.
408 Correspondence: Susanna Bodoy, Institute for Research in Biomedicine Barcelona,
409 Baldiri Reixac, 12, Barcelona 08028, Spain; e-mail:
410 susanna.bodoy@irbbarcelona.org; Manuel Palacín, Institute for Research in
411 Biomedicine Barcelona, Baldiri Reixac, 12, Barcelona 08028, Spain; e-mail:
412 manuel.palacin@irbbarcelona.org.
413 **Acknowledgements**
414 This work was supported by grants from the Spanish Ministry of Science and
415 Innovation (grant SAF2015-64869-R-FEDER and RTI2018-094211-B-100), Ramon
416 Areces Fundation (I.O.F.R.ARECES) and the Generalitat de Catalunya (grant 2017
417 SGR 961). Grant RTI2018-101735-B-I00 from the Spanish Ministry of Science and
418 Innovation to MS. The EMBO Short Term Fellowship Program facilitated the
419 collaboration between international groups. We are also grateful to Dr. Angel Nebreda
420 at the IRB Barcelona, Spain, for *LysM-Cre* transgenic mice; Dra Anna Bigas from
421 IMIM, Spain, for CD45.1 mice. We thank Jorge Seco and Vanessa Hernández for
422 technical assistance and help with the experimental animals, and the Daniel Bravo
423 Foundation for support with amino acid determination.
424
425
426
427
428
429

Figure 1

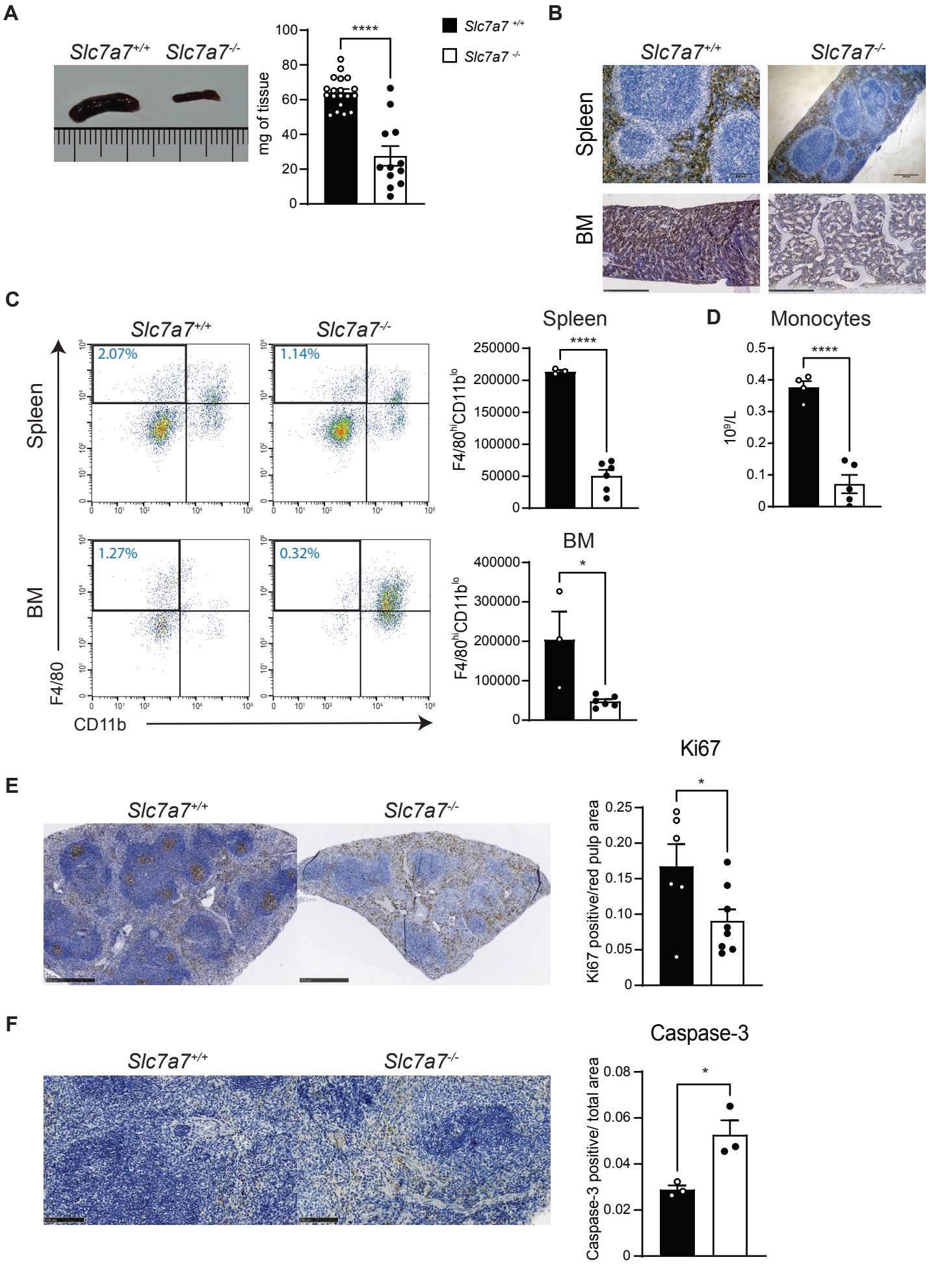

Figure 1. y^+LAT1 conditional knockout mice present a drastic reduction of BMMs and RPMs. (A) *Slc7a7*$^{-/-}$ mice and its control littermates were dissected, and spleens were photographed (left panel). Spleen weights are indicated on the right panel. (B) Representative immunohistochemistry staining of F4/80$^+$ cells in the spleen and bone marrow (BM) from *Slc7a7*$^{+/+}$ and *Slc7a7*$^{-/-}$ animals. Spleen scale bar, 200 µm, bone marrow scale bar, 500 µm. (C) Flow cytometry quantification of total number of red pulp macrophages per spleen and bone marrow macrophages per femur and tibia (CD11b^{lo}, F4/80^{hi}). (D) Comparison of peripheral blood concentration of circulating monocytes levels. (E) Representative Ki67 staining of spleen of *Slc7a7*$^{+/+}$ and *Slc7a7*$^{-/-}$ mice (left) and its quantification (right). Scale bar, 500 µm. (F) Representative Active Caspase-3 staining of spleen of *Slc7a7*$^{+/+}$ and *Slc7a7*$^{-/-}$ mice (left) and its quantification (right). Scale bar,100 µm. Data are mean ± SEM. * $P \leq 0.05$, *** $P \leq 0.001$, **** $P \leq 0.0001$ between genotypes. *P* values were calculated using two-tailed *t*-test.

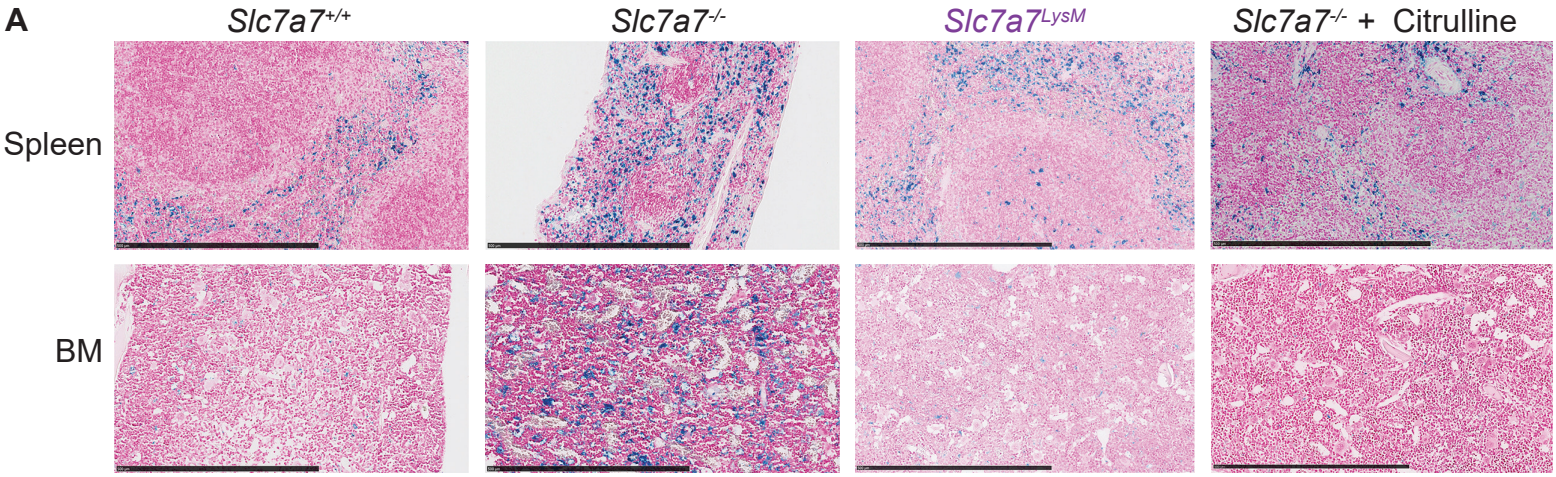

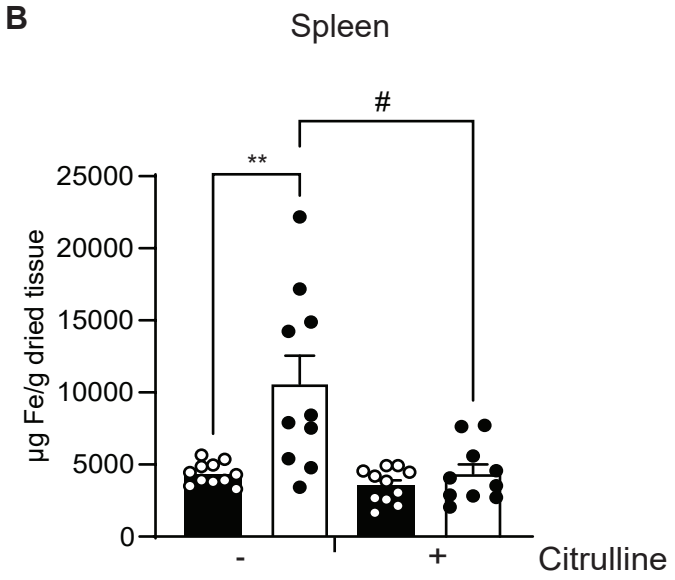

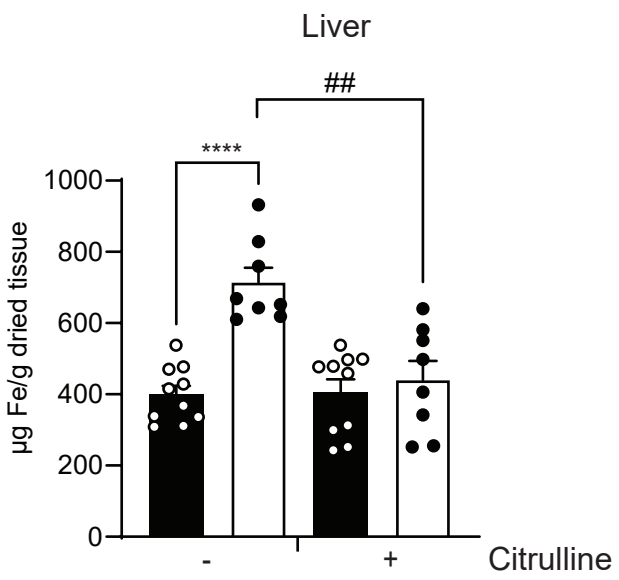

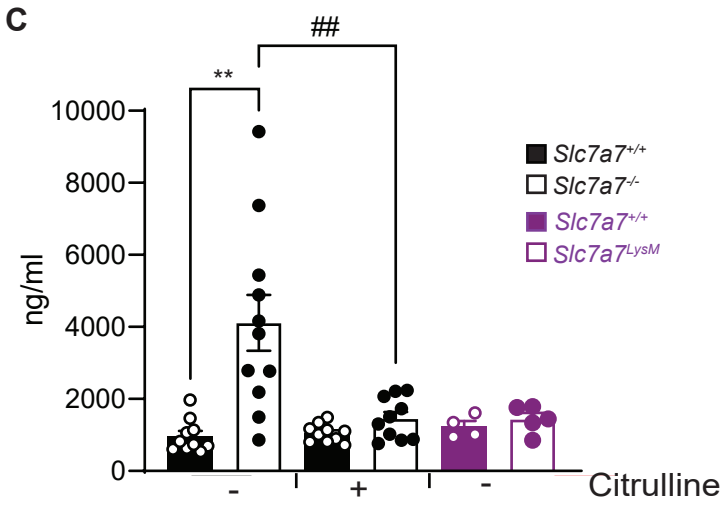

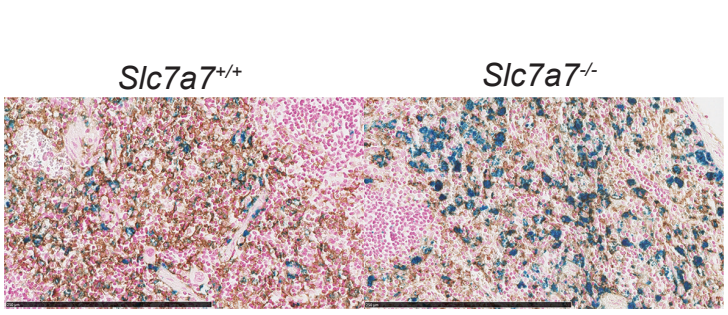

Figure 2. *Slc7a7* $^{-/-}$ RPMs show increased iron accumulation and exacerbated iron metabolism. (A) Representative iron Perl's Prussian Blue staining of spleens and bone marrow (BM) from indicated genotype supplemented or not with citrulline (1 g/L of drinking water). Scale bars, 500 µm. (B) Total non-heme iron content from spleen (left panel) and liver (right panel) from *Slc7a7*$^{+/+}$ and *Slc7a7*$^{-/-}$ mice. (C) Plasma ferritin quantification of indicated genotype supplemented or not with citrulline. (D) F4/80 (brown) and iron (blue) staining of spleen sections of indicated genotype. Scale bar, 250 µm. Data are mean ± SEM. ** $P \leq 0.01$, *** $P \leq 0.001$ between genotypes. $^{\#}$ $P \leq 0.05$, $^{\#\#}$ $P \leq 0.01$ vs. *Slc7a7*$^{-/-}$ mice without citrulline. *P* and # values were calculated using two-tailed *t*-test.

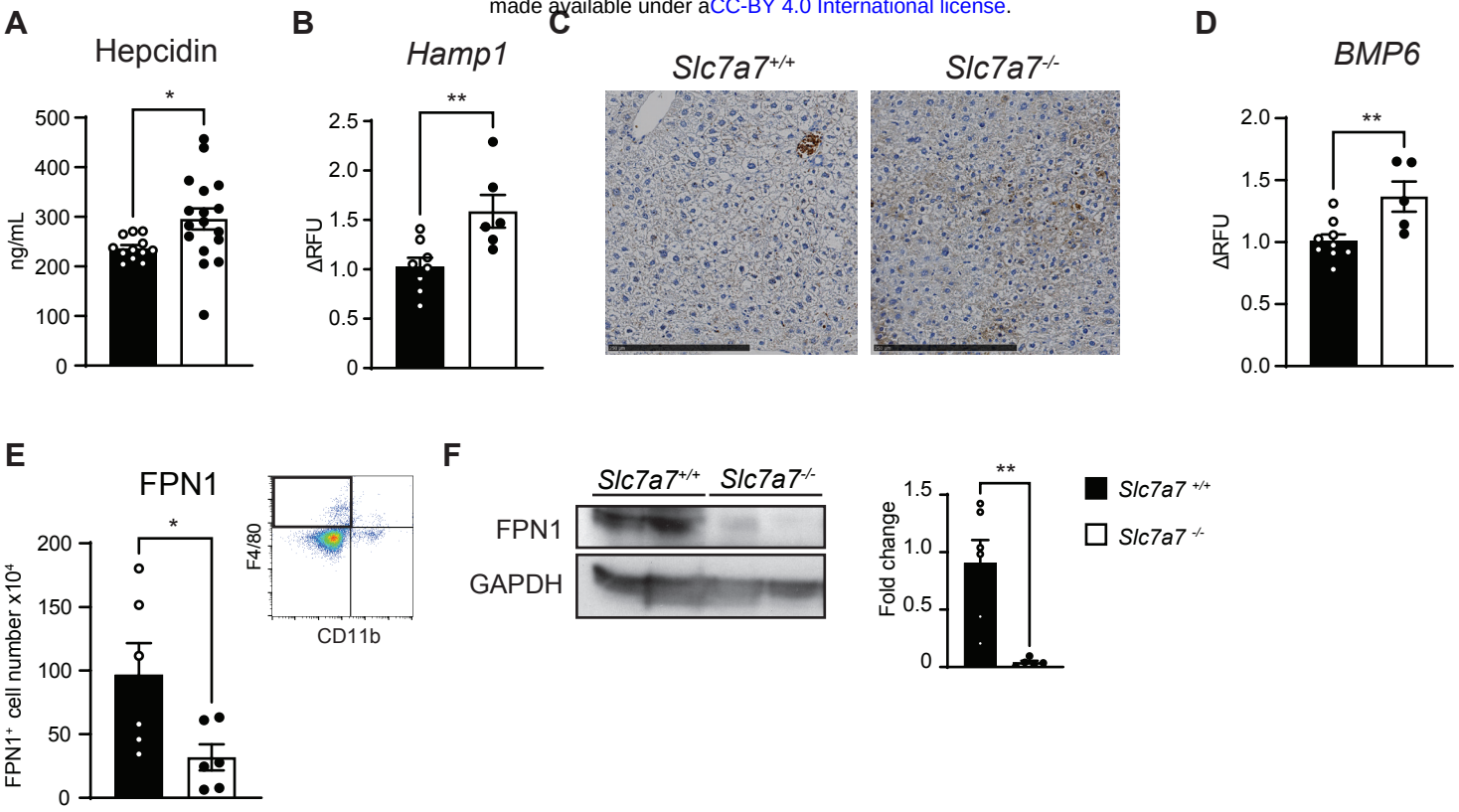

Figure 3. Total loss of *Slc7a7* results in decreased FPN1 expression. (A) Plasma hepcidin levels in *Slc7a7*$^{+/+}$ and *Slc7a7*$^{-/-}$ mice. (B) *Hamp1* mRNA levels (i.e., gene encoding for hepcidin) of *Slc7a7*$^{+/+}$ and *Slc7a7*$^{-/-}$ mice livers. (C) Iron histology by enhanced Pearl's Prussian blue (brown) staining of liver sections of indicated genotype. Scale bar, 250 μm . (D) *BMP6* mRNA expression of *Slc7a7*$^{+/+}$ and *Slc7a7*$^{-/-}$ mice livers. (E) Absolute cell number of CD11b^{lo}, F4/80^{hi}, FPN1^{hi} per spleen and representative FACS plot showing selected gate. (F) FPN1 protein expression in spleen membranes of the indicated genotypes. Quantification is expressed as FPN1/GAPDH fold change. Data are represented as mean ± SEM. * $P \leq 0.05$, ** $P \leq 0.01$ between genotypes. *P* values were calculated using two-tailed *t*-test.

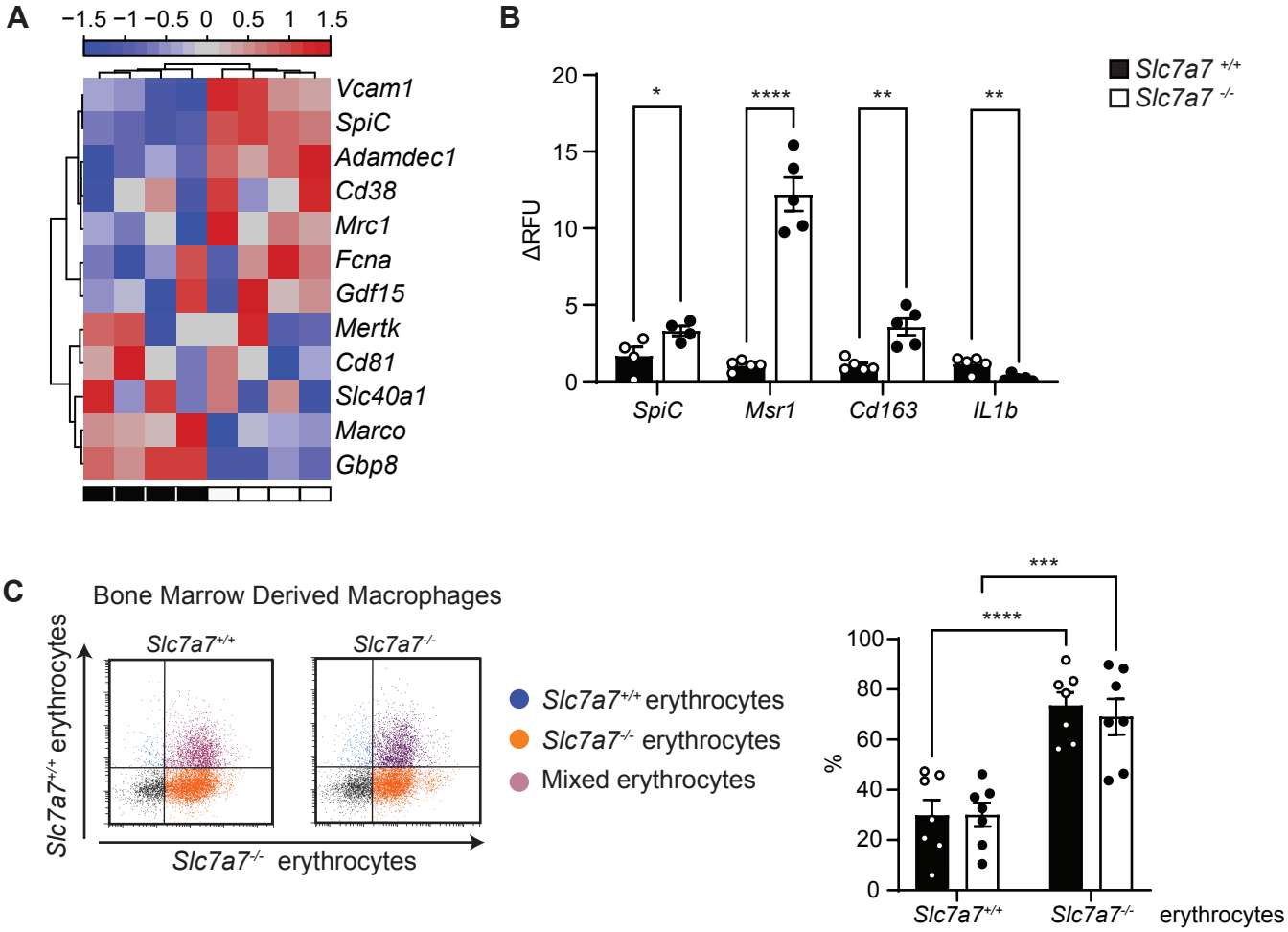
A
−1.5 −1 −0.5 0 0.5 1 1.5
Vcam1
SpiC
Adamdec1
Cd38
Mrc1
Fcna
Gdf15
Mertk
Cd81
Slc40a1
Marco
Gbp8
B
Slc7a7 +/+
Slc7a7 -/-
ΔRFU
20
15
10
5
0
*
****
**
**
SpiC
Msr1
Cd163
IL1b
C
Bone Marrow Derived Macrophages
Slc7a7+/+
Slc7a7-/-
Slc7a7+/+ erythrocytes
Slc7a7-/- erythrocytes
Slc7a7-/- erythrocytes
Slc7a7+/+ erythrocytes
Slc7a7-/- erythrocytes
Mixed erythrocytes
***
****
%
100
80
60
40
20
0
Slc7a7+/+
Slc7a7-/-
erythrocytes

Figure 4. y^+LAT1 ablation leads to increased erythrophagocytosis. (A) RPMs ($F4/80^{hi}CD11b^{lo}$) were sorted and gene expression analysis was carried out using the Affymetrix platform and a selection of RPM-associated genes(Haldar et al., 2014; Kohyama et al., 2009) was plotted as a heat map. Black boxes indicate the *Slc7a7*$^{+/+}$ genotype and empty boxes the *Slc7a7*$^{-/-}$ genotype. (B) Quantitative RT-PCR analysis of mRNA expression levels of indicated genes related to erythrophagocytosis and differentiation in RPM of *Slc7a7*$^{+/+}$ and *Slc7a7*$^{-/-}$ mice. (C) Erythrophagocytosis assay. Briefly, BMDMs were co-incubated with previously labelled erythrocytes. *Slc7a7*$^{+/+}$ erythrocytes (blue circles) were labelled with CellVue Claret, while *Slc7a7*$^{-/-}$ erythrocytes (orange circles) were labelled with PKH26. Left: Representative dot plots show the gating strategy for the erythrophagocytosis assay. Right: Percentage of the cell populations analyzed. Filled bars and empty bars represent *Slc7a7*$^{+/+}$ and *Slc7a7*$^{-/-}$ macrophages, respectively. Data are mean ± SEM. * $P \leq 0.05$, ** $P \leq 0.01$, *** $P \leq 0.001$, **** $P \leq 0.0001$ between genotypes. *P* values were calculated using two-tailed *t*-test.

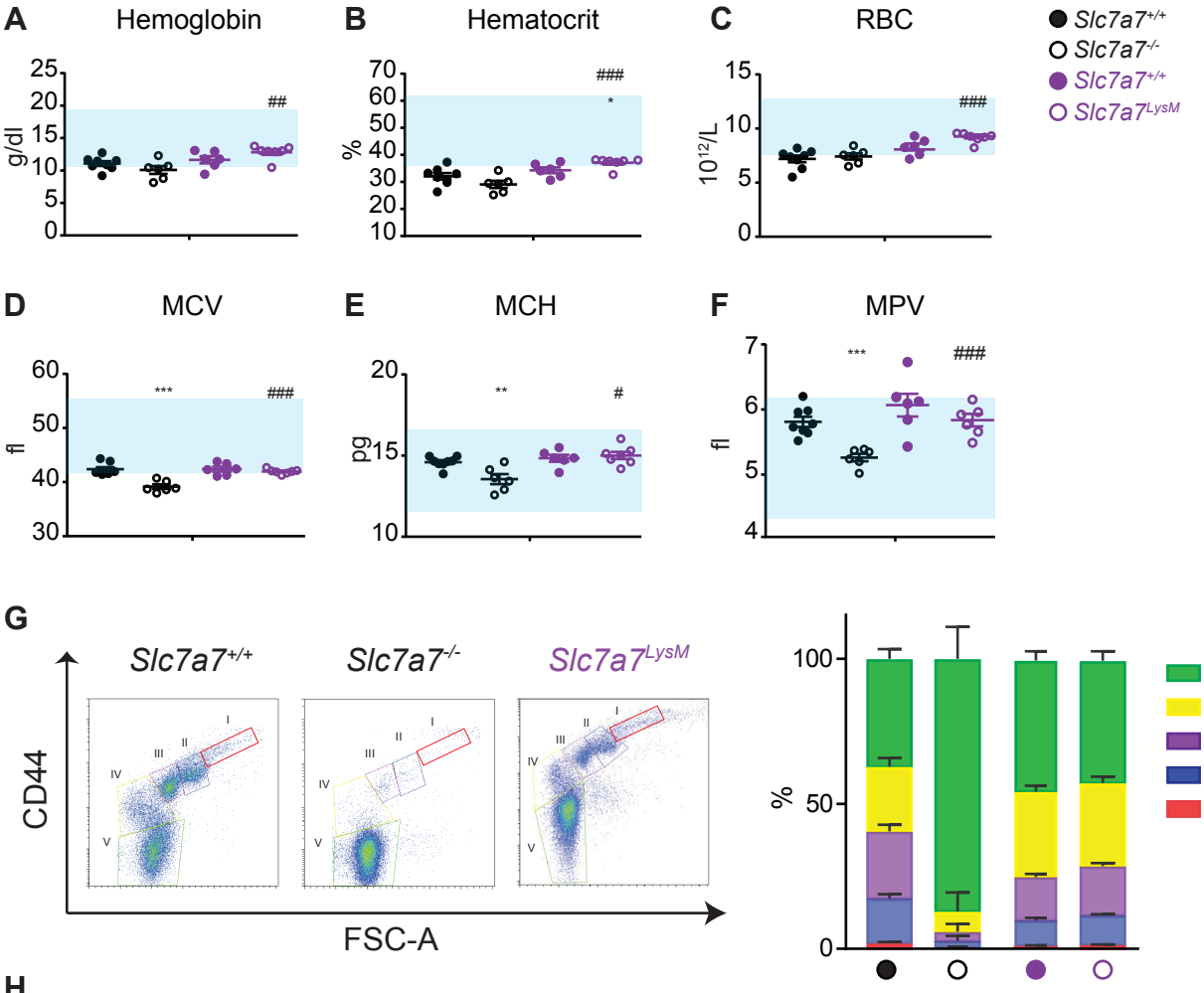

Figure 5. y^+LAT1 depletion results in defective erythropoiesis. (A-F) Quantification of blood hemoglobin (A), hematocrit (B), RBC concentration (C), mean corpuscular volume (D), mean corpuscular hemoglobin (E) and mean platelet volume (F) of indicated genotype. (G) Left: Representative dot plots show the gating strategy for erythroid progenitors (V, IV, III, II and I) (Chen et al., 2009) from indicated genotype. Briefly, cells were first gated in $TER119^+$ and further separated by CD44 versus Forward Scatter (FSC-A). Right: Percentage of the cell populations analyzed. (H) Plasma erythropoietin levels in *Slc7a7*$^{+/+}$ and *Slc7a7*$^{-/-}$ mice fed with a low protein diet. Data are mean ± SEM. All experiments were performed independently at least twice. * $P \leq 0.05$, ** $P \leq 0.01$, *** $P \leq 0.001$ between genotypes. *P* values were calculated using two-tailed *t*-test.

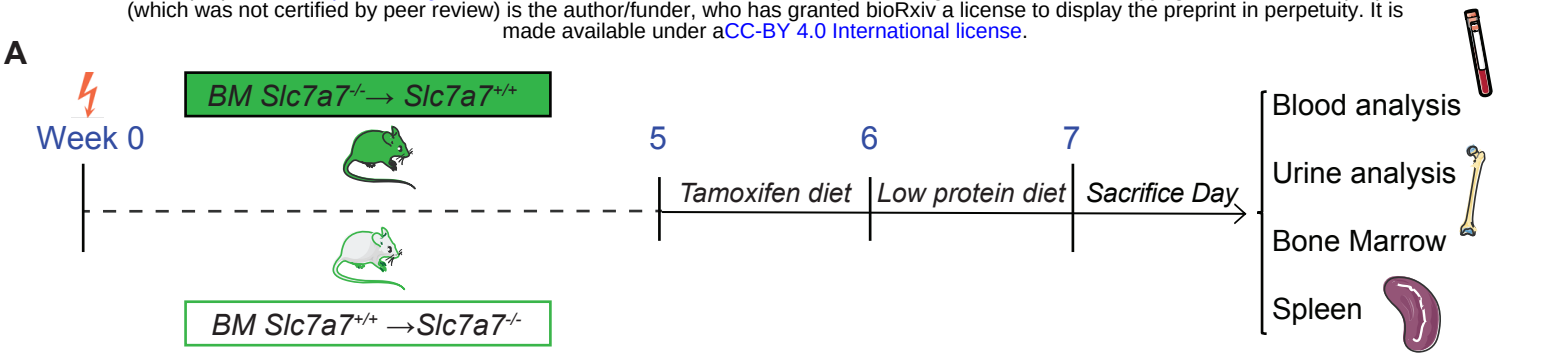

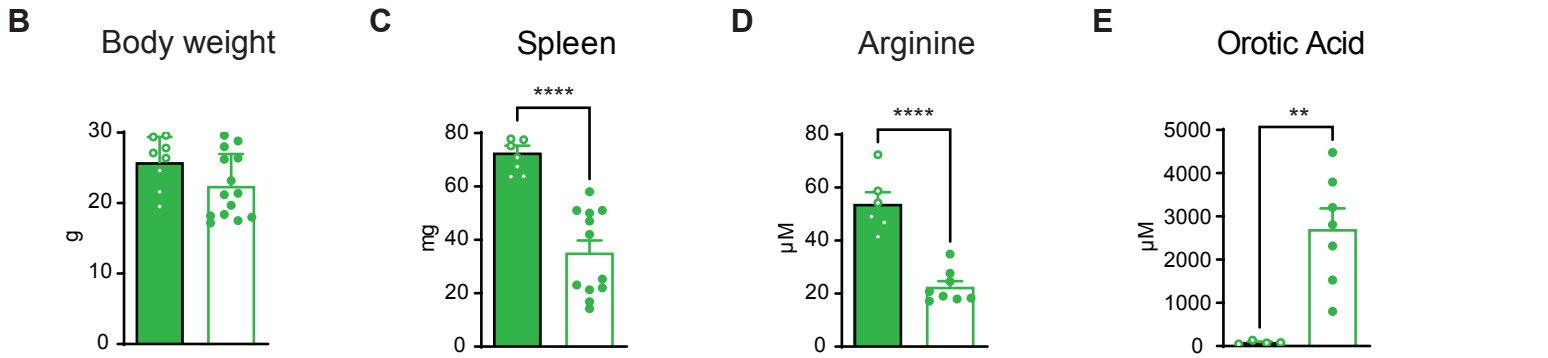

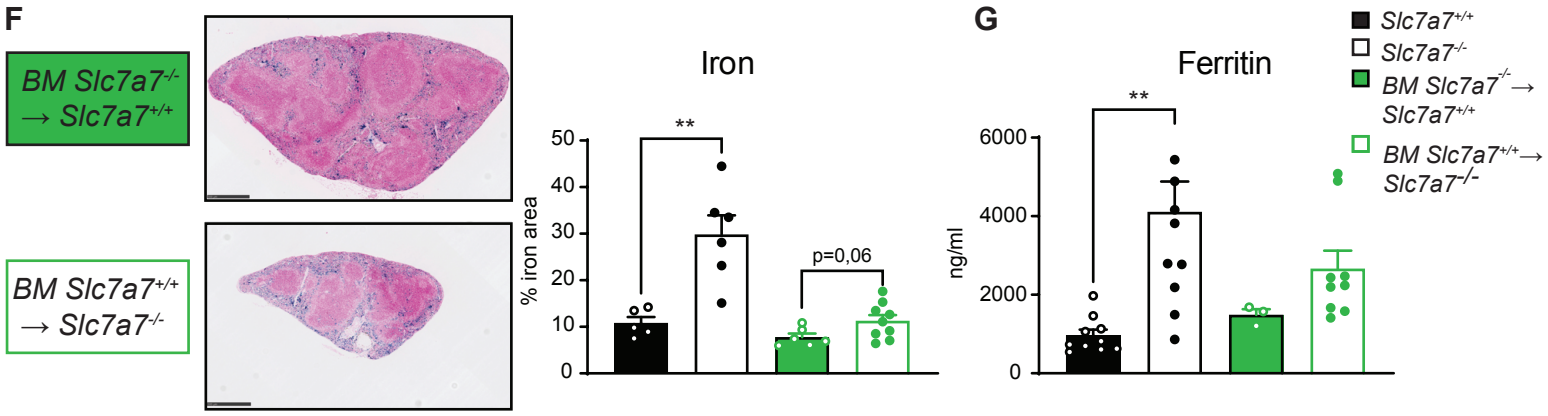

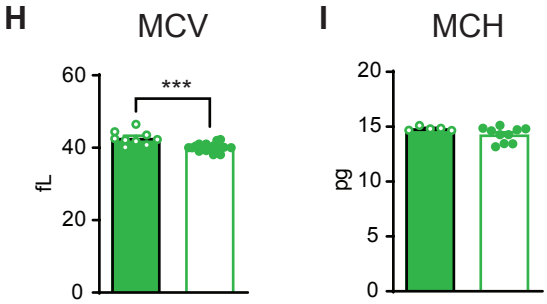

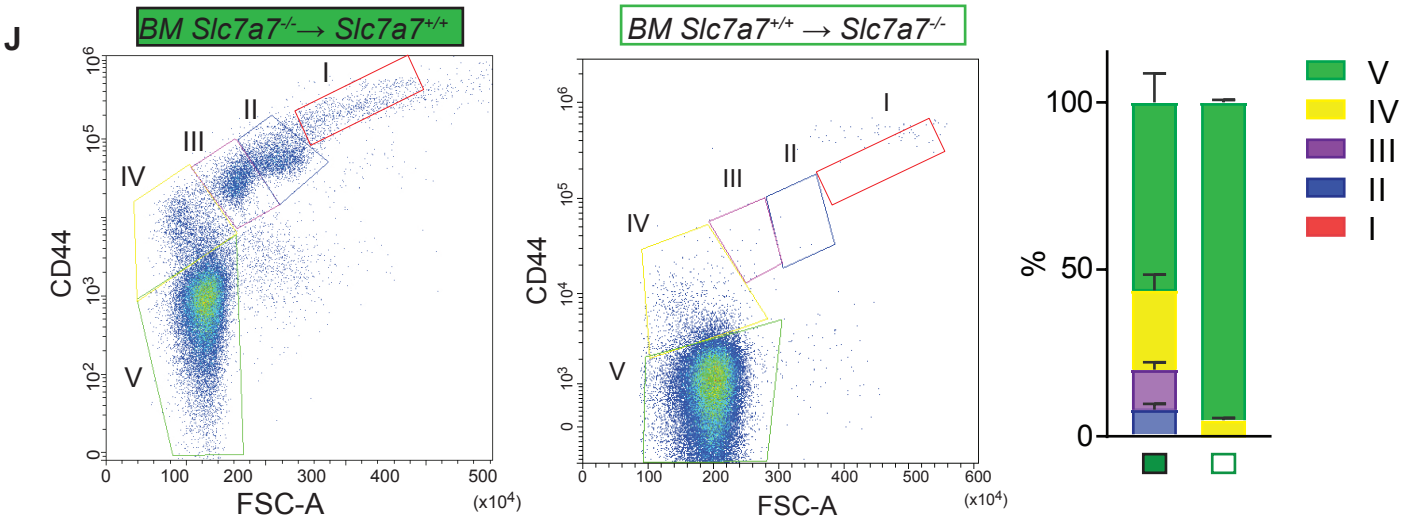

Figure 6. Iron accumulation but not defective hematopoiesis and metabolic derangement improves after bone-marrow transplant. (A) 5 weeks after transplant, mice were first fed a tamoxifen diet for 1 week and then a low-protein diet for 10 days prior to sacrifice day. (B-E) Body weight (B), spleen weight (C), plasma arginine (D), and urine orotic acid (E) of *Slc7a7*$^{-/-}$ mice transplanted with wild-type CD45.2 bone marrow (BM *Slc7a7*$^{+/+}$ → *Slc7a7*$^{-/-}$) and *Slc7a7*$^{+/+}$ mice transplanted with *Slc7a7*$^{-/-}$ CD45.1 bone marrow (BM *Slc7a7*$^{-/-}$ → *Slc7a7*$^{+/+}$). (F) Left: Isolated spleens of the indicated genotypes were embedded in paraffin for histopathological examination (Perl's Prussian Blue). Scale bar, 500 µm. Right: Percentage of iron area in the indicated genotypes and transplanted mice. (G) Plasma ferritin levels in *Slc7a7*$^{+/+}$ and *Slc7a7*$^{-/-}$ mice, and *Slc7a7*$^{-/-}$ and Slc*7a7*$^{+/+}$ mice transplanted with wild-type BM and *Slc7a7*$^{-/-}$ BM, respectively. (H-I) Hematological analysis (MCV, mean corpuscular volume; MCH, mean corpuscular hemoglobin) of *Slc7a7*$^{-/-}$ mice transplanted with wild-type CD45.2 bone marrow and *Slc7a7*$^{+/+}$ mice transplanted with *Slc7a7*$^{-/-}$ CD45.1 bone marrow. (J) Left: Representative dot plots show the gating strategy for erythroid progenitors (V, IV, III, II and I) (Chen et al., 2009) of *Slc7a7*$^{-/-}$ mice transplanted with wild-type BM and *Slc7a7*$^{+/+}$ mice transplanted with *Slc7a7*$^{-/-}$ bone marrow. Left: Boxes in the flow cytometry plots represents I-IV erythroblasts populations. Right: Percentage of the cell populations analyzed. Data are mean ± SEM. All experiments were performed independently at least twice. * $P \leq 0.05$, ** $P \leq 0.01$, *** $P \leq 0.001$, **** $P \leq 0.0001$ between genotypes. *P* values were calculated using two-tailed *t*-test.

Supplementary Figure 1

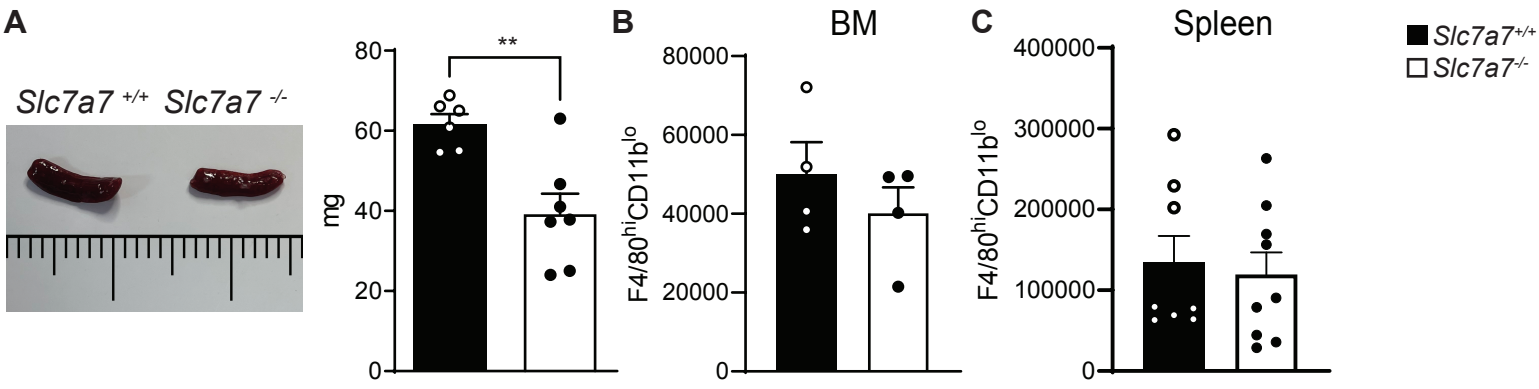

Supplementary Figure 1. *Slc7a7* $^{-/-}$ mouse model treated with citrulline improve spleen weight and recover BMMs and RPMs number. (A) *Slc7a7*$^{-/-}$ mice and its control littermates treated with citrulline in the drinking water (1g/L) were dissected, and spleens were photographed (left panel). Spleen weights are indicated on the right panel. (B) Flow cytometry quantification of total number of bone marrow (BM) macrophages and red pulp macrophages (C) per femur and tibia (CD11b^{lo}, F4/80^{hi}). Data are mean ± SEM. ** $P \leq 0.01$ between genotypes. *P* values were calculated using two-tailed *t*-test.

Supplementary Figure 2

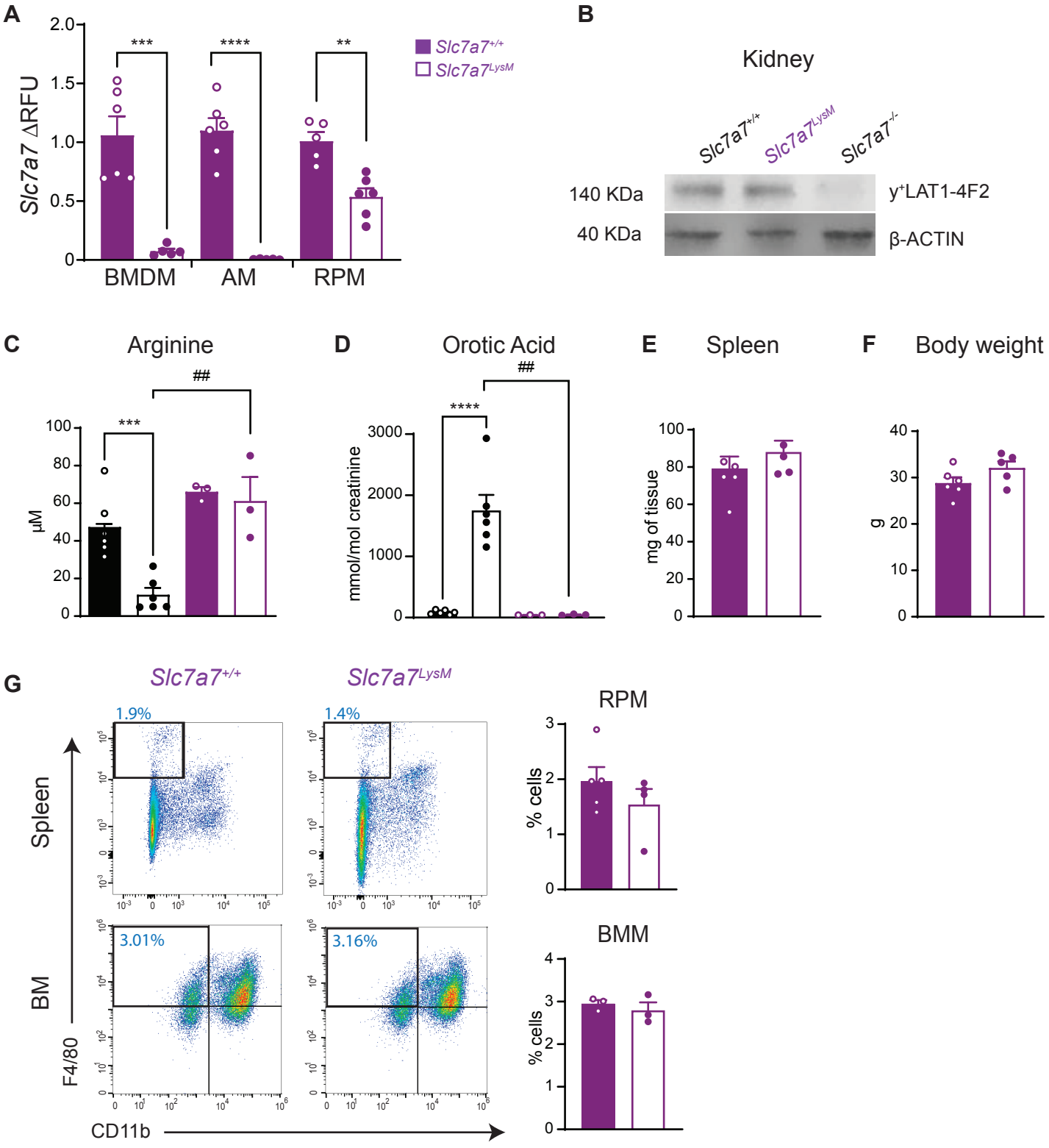

Supplementary Figure 2. y^+LAT1 deficiency in myeloid cell line does not reproduce the deficiencies of the conditional knockout mouse. (A) mRNA expression of *Slc7a7* gene in BMDMs, AMs and RPMs from *Slc7a7*$^{LysM-/-}$ and their control. (B) y^+LAT1 protein expression of kidney membranes in the indicated genotypes. (C) Plasma arginine, (D) urine orotic acid, (E) spleen and (F) body weight of *Slc7a7*$^{+/+}$, *Slc7a7*$^{-/-}$, *Slc7a7*$^{LysM-/-}$ mice and their control counterparts. (G) Flow cytometry analysis with the indicated markers on BMs and splenocytes of the designated genotypes. The percentage of CD11b^{lo}F4/80^{hi} is shown (right panel). Data are mean ± SEM. ** $P \leq 0.01$, *** $P \leq 0.001$ between genotypes. $^{\#}$ $P \leq 0.05$, $^{\#\#}$ $P \leq 0.01$ vs. *Slc7a7*$^{-/-}$ mice. *P* values were calculated using two-tailed *t*-test.

Supplementary Figure 3

A

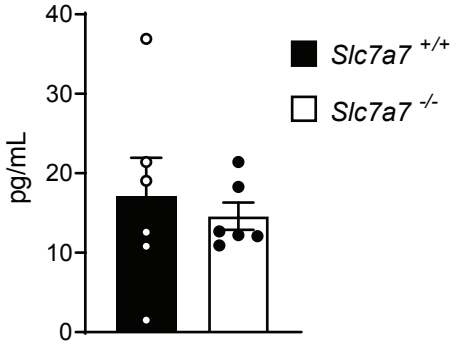

B

Hallmark Term	PValue	NES
UV response DN	0.001	2.584
Xenobiotic metabolism	0.044	2.025
Complement	0.026	1.883
Wnt-β catenin signaling	0.012	1.855
Protein secretion	0.043	1.624
G2M checkpoint	0	-3.917
IL2 STAT5 signaling	0	-3.311
Mitotic spindle	0	-3.07
Inflammatory response	0	-3.049
IL6 JAK STAT3 signaling	0	-2.797
TNF-α signaling via NFKB	0.001	-2.599
Interferon γ response	0.001	-2.584
Allograft rejection	0	-2.569
Estrogen response late	0.007	-2.518
KRAS signaling up	0.007	-2.509
E2F Targets	0	-2.469
Angiogenesis	0.005	-2.263
Apoptosis	0	-2.132
Apical Junction	0.009	-2.13
Unfolded protein response	0.009	-2.099
Estrogen response early	0.017	-1.981
Glycolysis	0.054	-1.975
mTORC1 SIGNALING	0.033	-1.913
P53 Pathway	0.094	-1.637
Fatty acid metabolism	0.131	-1.557
Heme metabolism	0.187	-1.412

Supplementary Figure 3. IL6 plasma levels and broad hallmarks patways

(A) Plasma IL6 levels of *Slc7a7*$^{+/+}$ and *Slc7a7*$^{-/-}$ mice. Data are mean ± SEM. *P* values were calculated using two-tailed *t*-test. (B) The most significative pathways in *Slc7a7*$^{-/-}$ red pulp macrophages, Pvalue and Normalized Enrichment Score (NES) values are shown.

MATERIALS AND METHODS

Data and code availability

Microarray data has been deposited in a public repository and the accession numbers is GSE164827.

Animals

All animal work was approved and conducted according to guidelines established. This project (DARP n°9177) has been assessed favourably by the Institutional Animal Care and Use Committee from Parc Científic de Barcelona (IACUC-PCB) and the IACUC considers that the above-mentioned project complies with standard ethical regulations and meets the requirements of current applicable legislation (RD 53/2013 Council Directive; 2010/63/UE; Order 214/1997/GC). C57BL/6 mice were purchased from Harlan Europe. *Slc7a7*$^{loxp/loxp}$ mice were generated by Eurogentec. To generate *Slc7a7*$^{-/-}$ and *Slc7a7*^{LysM} mice, *Slc7a7*$^{loxp/loxp}$ were crossed with UBC-Cre-ERT2 mice from The Jackson Laboratory and LysM-Cre provided by Dr. Ángel R. Nebreda, respectively. Male or female mice of 12 weeks old were used. Mice were housed in groups of 2-5 animals per cage and were kept under a 12 h dark-light period. Food and water were supplied *ad libitum*. Animals were fed a standard diet (Teklad global 14% protein rodent maintenance diet) until tamoxifen induction, which consisted of a tamoxifen diet for one week. After the induction period, animals were kept on a low-protein diet for 7-10 days, supplemented or not with 1g/l L-citrulline in drinking water. Control and *Slc7a7*$^{-/-}$ littermates on a C57Bl6/J genetic background were sacrificed at 10-12 weeks of age by cervical dislocation. Tissues were dissected and flash-frozen in liquid nitrogen for RNA, protein, and iron quantification studies. For histological analysis, mice were anesthetized with ketamine and xylazin (respectively 1 mg and 0.1 mg per 10 g of body weight, i.p., respectively) and subjected to transcranial

674 perfusion. For hematological and biochemical studies, EDTA or heparin blood was
675 collected from cardiac puncture. Bone marrow was flushed out from femur and tibia
676 bones.
677 Mice carrying the myeloid-specific knockout of the *Slc7a7* gene (*LysM*$^{Cre/+}$
678 *Slc7a7*$^{flox/flox}$) were sacrificed at 12 weeks of age, and only those with more than 80%
679 deletion of endogenous protein were used for the experiments.
680 ***Bone marrow transplantation (BMT)***
681 Recipient mice were lethally irradiated (9.5Gy) and transplanted with 2x10^6 bone
682 marrow (BM) cells by retro-orbital injection (Bennett et al., 2018). For the re-population
683 experiments, total BM cells from either *Slc7a7*$^{-/-}$ (CD45.2) or *Slc7a7*$^{+/+}$ (CD45.1) mice
684 were transplanted into lethally irradiated B6 recipient mice (CD45.1 or CD45.2). As a
685 follow-up step, five weeks after transplantation to allow whole body hematopoiesis
686 regeneration, mice were subjected to tamoxifen diet for 7 days, and then treated with
687 a low-protein diet for 10 days prior to the sacrifice. BM reconstitution was monitored
688 by flow cytometry.
689 γ-Irradiation of mice was performed in a 137Cs-γ IBL 437C H irradiator (Shering CIS
690 bio international) at 2.56Gy/min rate for the indicated dosage. The irradiated mice were
691 inspected daily. Mice were given *Baytril* water containing antibiotics (Bayer, Shawnee
692 Mission, JS) for at least 30 days to reduce the probability of infection from opportunistic
693 pathogens.
694 ***Flow cytometry and cell sorting***
695 For the analysis of splenocytes and bone marrow cells, crushed spleens and flushed
696 BM were isolated and incubated with Fc block (anti-mouse CD16/32; Thermofisher)
697 for 30 min on ice. Cell suspensions were stained for the expression of CD71; CD11b;
698 CD45.1; CD45.2 (BD Biosciences); CD34 (eBiosciences); F4/80; TER119; CD106

699 (BioLegend) for 30 min on ice. Flow cytometry analysis was performed on Gallios (BD
700 Boisciences). For spleen staining, crushed tissues were filtered through a 40 μM cell
701 strainer and erythroid cells were removed by incubation with ammonium-chloride-
702 potassium lysis buffer prior to Fc blocking. Cell sorting (purity > 90%) was carried out
703 using a FACS Aria II (BD Biosciences). For microarray analysis, spleens were
704 prepared as described above and stained with anti-CD106, anti-CD11b and anti-F4/80
705 (ThermoFisher) for purified RPMs.
706 Cell doublets were excluded from all analyses and, when possible, dead cells were
707 excluded by the use of DAPI. Data analysis was carried out using FlowJo™ Software.

708 ***In vitro erythrophagocytosis assay***

709 To prepare primary BMDMs, cells obtained from mouse femurs and tibia were cultured
710 for 7 days in the presence of L-Cell (L929 SN) in DMEM supplemented with 10% FBS,
711 penicillin (50 U/mL) and streptomycin (50 µg/mL). BMDMs were plated 24 hours prior
712 to the day of the experiment. On the day of the experiment, previously seeded BMDMs
713 were activated with lipopolysaccharide (100 ng/mL) for 2h and fresh RBCs were
714 extracted, washed and labelled with CellVue® or PKH26 following the manufacturer's
715 instructions. RBCs were then incubated with previously activated BMDMs for 2
716 minutes ($10 \cdot 10^6$ RBC/$1 \cdot 10^6$ BMDM) at 37ºC in a 5% CO_2 incubator. Macrophages
717 were washed twice with PBS and finally incubated with an erythrolysis buffer (R&D
718 Systems) to lyse non-ingested RBCs. Cells were then collected and analyzed by flow
719 cytometry.

720 ***Histological sample preparation and analysis***

721 Samples were fixed overnight at 4ºC with neutral buffered formalin. After fixation,
722 bone tissue (femur) was washed with PBS 1x and decalcified with Osteosoft® reagent

723 for a minimum 15 days at RT. All samples were embedded in paraffin. Paraffin-
724 embedded tissue sections (2-3 µm in thickness) were air-dried and further dried at 60
725 ºC overnight. Bone sections were maintained at 60ºC for 48 h.
726 For special staining, paraffin-embedded tissue sections were dewaxed and stained
727 with Iron Stain Kit to identify iron pigment using the Dako Autostainer Plus and
728 following the manufacturer instructions. When combining Iron staining with F4/80 IHC,
729 iron staining was done before following the described protocols.
730 Prior to immunohistochemistry, sections were dewaxed and therefore epitope retrieval
731 was performed using citrate buffer pH6 for 20 min at 121ºC with an autoclave or
732 proteinase K for 5 min at RT for anti-caspase 3 (Cell Signalling) and rat monoclonal
733 Anti-F4/80 (eBioscience), respectively. For rabbit polyclonal anti-Ki67 (Abcam)
734 sections were dewaxed as part of the antigen retrieval process using the low pH
735 EnVision™ FLEX Target Retrieval Solutions (Dako, Burlington) for 20min at 97ºC
736 using a PT Link (Dako, Agilent). Quenching of endogenous peroxidase was performed
737 by 10 min of incubation with Peroxidase-Blocking Solution at RT. Non-specific
738 bindings were blocked using 5 % of goat normal serum or normal donkey serum mixed
739 with 2.5 % BSA diluted in the wash buffer for 60 min at RT. The primary antibody
740 dilutions used were 1:300, 1:100 and 1:2000, for 120 min, overnight or 60 min,
741 respectively. The secondary antibody used was a BrightVision Poly-HRP-Anti Rabbit
742 IgG Biotin-free, ready to use or the secondary antibody used was a Biotin-SP (long
743 spacer) AffiniPure Donkey Anti-Rat IgG (H+L) at 1:500 (in wash buffer) for 60 min
744 followed by amplification with Streptavidin-Peroxidase polymer at 1:1000. Antigen–
745 antibody complexes were revealed with 3-3′-diaminobenzidine, with the same time
746 exposure (1 min). Sections were counterstained with hematoxylin and mounted with

Mounting Medium, Toluene-Free using a Dako CoverStainer. Specificity of staining was confirmed with rabbit IgG, polyclonal - Isotype control or Normal Rat IgG Control. Image acquisition. Brightfield images were acquired with a NanoZoomer-2.0 HT C9600 digital scanner (Hamamatsu) equipped with a 20X objective. All images were visualized with the NDP.view 2 U123888-01 software. All images were visualized with a gamma correction set at 1.8 in the image control panel of the NDP.view 2 U12388-01 software.

Prior to immunohistochemistry, for Ki67 sections were dewaxed as part of the antigen retrieval process using the low pH EnVision™ FLEX Target Retrieval Solutions (Dako, Burlington) for 20 min at 97ºC using a PT Link (Dako – Agilent). For caspase 3 samples were dewaxed and antigen retrieval treatment was performed with citrate buffer pH6 for 20 min at 121ºC with an autoclave. Quenching of endogenous peroxidase was performed by 10 min of incubation with Peroxidase-Blocking Solution (Dako REAL S2023). Rabbit polyclonal primary anti-Ki67 antibody (A. Menarini diagnostics – NCL-ki67p) was diluted 1:1000 with EnVision FLEX Antibody Diluent (K800621, Dako, Agilent) and incubated for 60 min at RT. The secondary antibody used was a BrightVision Poly-HRP-Anti Rabbit IgG Biotin-free, ready to use (Immunologic, DPVR-110HRP). Antigen–antibody complexes were revealed with 3-3′-diaminobenzidine, with the same time exposure per antibody (3 and 5 min respectively). Sections were counterstained with hematoxylin and mounted with Mounting Medium, Toluene-Free using a Dako CoverStainer.

Amino acid content

Briefly, amino acids were determined by ion exchange chromatography with ninhydrin derivatization and spectrometric detection (Biochrom 30, Chromsystems, Cambridge, UK). Plasma (300 µL) were deproteinized with sulphosalicylic acid containing L-

norleucine as internal standard (final concentration 100 µmol/L). After centrifugation, 200 µL of supernatant were adjusted to pH = 2.1 with lithium hydroxide, and then, injected onto the liquid chromatograph. Urinary orotic acid was analyzed following a spectrometric procedure (458 nm), by reacting with para-dimethylaminobenzaldehyde.

Tissue iron content

Liver and spleen non-heme iron content was measured using the bathophenanthroline colorimetric method. Mouse tissues were dried at 45ºC for 3 days, weighted, and digested for 48 h at 65ºC in 10% TCA/10% HCl to allow deproteinization of non-heme iron. Diluted extracts were added to a 0.01% bathophenanthroline disulfonic acid, 0.1% thioglycolic, 7M sodium acetate solution and the absorbance at 535 nm was measured using a spectrophotometer Ultrospec 3100pro (Amersham Biosciences). The iron content of samples was obtained by interpolation from a standard curve and calibrated to the weight of dried material (Jd and Th, 1968; Patel et al., 2002).

Plasma measurements

ELISA kit was used to determine the IL6 (Abnova), hepcidin (Intrinsic Life Science), ferritin (Abcam) and erythropoietin (R&D Systems) proteins in fresh plasma. The procedures were done following the manufacturer's instructions.

Microarray analysis

For gene expression analysis of RPMs, total RNA was isolated from previously purified cells using magnetic beads and the Agencourt RNA Clean XP kit (Beckman Coulter). Quality and quantity were assessed using a Bioanalyzer 2100 (Agilent Technologies, Palo Alto, CA). Library preparation and amplification were performed as described previously by (Gonzalez-Roca et al., 2010). RNA was amplified for 22 cycles and

purified using PureLink Quick PCR Purification kit (Invitrogen) in the Genomic Facility of IRB Barcelona.

Pre-processing of microarray data

Microarray datasets were processed separately using R (R Core, 2019) packages affy (Gautier et al., 2004) and affyPLM (Bolstad et al., 2005) from Bioconductor (Gentleman et al., 2004). Raw cell files data were processed using RMA (Irizarry, 2003) and annotated using the information available on the Affymetrix – Thermofisher web page. Standard quality controls were performed in order to identify abnormal samples regarding: a) spatial artefacts in the hybridization process (scan images and pseudo-images from probe level models); b) intensity dependences of differences between chips (MvA plots); c) RNA quality (RNA digest plot); d) global intensity levels (boxplot of perfect match log-intensity distributions before and after normalization and RLE plots); and e) anomalous intensity profile compared to the rest of the samples (NUSE plots, Principal Component Analysis).

Differential expression

A differential expression analysis was performed for *Slc7a7*$^{+/+}$ and *Slc7a7*$^{-/-}$ comparisons using a linear model with empirical shrinkage (Smyth, 2004) as implemented in Limma R package (Ritchie et al., 2015). This model included the batch of scanning for statistical control. Adjustment by multiple comparisons was performed using the Benjamini-Hochberg method (Benjamini and Hochberg, 1995).

Biological enrichment analysis

Genes quantified in the microarray experiment were annotated according to the Broad Hallmark (Liberzon et al., 2015) gene sets collection. Broad Hallmark sets were

819 translated to mouse homologous genes using the R package biomaRt (Durinck et al.,
820 2009).
821 Functional enrichment analyses were performed using a modification of ROAST (Wu
822 et al., 2010), a rotation-based approach implemented in the R package limma (Ritchie
823 et al., 2015) that is especially suitable for small size experiments. Such modifications
824 were implemented to accommodate in the ROAST algorithm the statistical re-
825 standardization proposed in (Efron and Tibshirani, 2007), which enables its use for
826 competitive testing (Goeman and Bühlmann, 2007). The MaxMean (Efron and
827 Tibshirani, 2007) statistic was used for testing geneset enrichment of Broad Hallmark.
828 For each gene, the most variable probeset within each gene was used in these
829 analyses (median absolute deviation).
830 The results of these analyses were adjusted by multiple comparisons using the
831 Benjamini-Hochberg False Discovery Rate method (Benjamini and Hochberg, 1995).
832 ***Clustering and visualization***
833 Gene expression of selected genes was graphically represented in a heatmap with the
834 heatmap R package, using a blue to red gradation, where red indicated the highest
835 expression and blue corresponded to the lowest expression values. Previously, the
836 expression data were summarized to the gene level using the most variable probeset
837 mapping to the same gene (median absolute deviation), and expression values were
838 centered and scaled gene-wise. Genes and samples were clustered using the Ward
839 agglomeration method and the correlation and Euclidean distances, respectively. To
840 gain clarity in the graphic, the most extreme values were truncated to -1.5 and 1.5.
841 All analyses were carried out using R and Bioconductor.
842 ***RNA extraction and quantitative real-time PCR***

Mice were killed by cervical dislocation, and tissues were immediately frozen for RNA isolation. Total mRNA was extracted from BMDMs or AMs using the Rneasy Total RNA Isolation kit (Qiagen, Alameda, CA, USA), following the manufacturer's instructions. RNA concentrations were measured with Nanodrop ND-1000 (ThermoFisher Scientific). Reverse transcription was performed with total RNA (2 ng) using the qScript cDNA SuperMix (Quantabio) following the manufacturer's instructions. PCRs were performed using the ABI Prism 7900 HT real-time PCR machine (Applied Biosystems, USA) and the SYBR® Green PCR Master Mix. Gene expression levels were normalized with β-actin as housekeeping genes. Primers used are listed in Supplementary table 1.

Protein isolation and western blot

Membrane proteins from cell cultures or tissues were extracted with Lysis buffer (25 mM Hepes, 4 mM EDTA, 250 mM Sucrose) containing protease inhibitor (1:000; Protease Inhibitor Cocktail Set III, EDTA-Free, Calbiochem). Briefly, tissues were lysed using the Tissue Lyser (Mini-beadbeater-16, Biospecproducts) and further centrifuged at 10000 g for 10 minutes at 4ºC. After centrifuging, the supernatant was centrifuged again on an ultracentrifuge at 55000 rpm for 1 hour at 4ºC. Finally, protein concentration was determined using Pierce BCA Protein Assay Kit (ThermoFisher Scientific). Membrane proteins were resolved in 10% acrylamide gels for SDS-PAGE and transferred to Immobilon membranes (Millipore). The following antibodies were used: polyclonal rabbit anti-y^+LAT1 was used at 1:750 dilution with 5% non-fat dried milk in PBS Tween-20 (0.1%) (Bodoy et al., 2019); rabbit anti-FPN1 was used at 1:250 dilution with 5% non-fat dried milk in TBS Tween-20 (0.1%) (Nairz et al., 2013). Antibody binding was then detected using appropriate horseradish peroxidase (HRP)-

867 conjugated secondary antibodies (1:1000 dilution). Proteins were detected by the
868 enhanced chemiluminescence method (GE Healthcare Life Sciences) and quantified
869 by scanning densitometry.

870 ***Primary bone marrow macrophages (BMDMs) cell culture***

871 BM cells from 12-week-old mice (either female or male) were flushed from mice femurs
872 and tibias. The cell suspension was lysed for 5 min in ACK lysis buffer at RT and then
873 washed, resuspended, and cultured for 7 days in Dulbecco's Modified Eagle Medium
874 (DMEM) supplemented with 10% heat-inactivated fetal bovine serum (FBS), 50 U/mL
875 penicillin, 50 µg/mL streptomycin and 50 ng/mL of recombinant M-CSF (Peprotech) or
876 30% of L-Cell (L929 supernatant (SN)) media. Six days after the seeding, cells were
877 harvested and re-seeded with the specific conditioned media for 24 hours. To deplete
878 arginine, arginine-free media was used (DMEM for SILAC, ThermoFisher).

879 **QUANTIFICATION AND STATISTICAL ANALYSIS**

880 Data were analyzed using GraphPad Prism Version 8 software. Statistical analysis
881 was performed using the Student's *t* test and one- and two-way ANOVA as specified
882 in each figure legend.

883

884 **References**

885 A-Gonzalez N, Quintana JA, García-Silva S, Mazariegos M, de la Aleja AG, Nicolás-ávila JA,
886 Walter W, Adrover JM, Crainiciuc G, Kuchroo VK, Rothlin C V., Peinado H, Castrillo A,
887 Ricote M, Hidalgo A. 2017. Phagocytosis imprints heterogeneity in tissue-resident
888 macrophages. *J Exp Med* **214**:1281–1296. doi:10.1084/jem.20161375
889 Al-Qattan S, Malcolmson C, Mercimek-Andrews S. 2021. Lysinuric protein intolerance
890 mimicking N-acetylglutamate synthase deficiency in a nine-year-old boy. *Mol Genet*
891 *Metab Reports* **27**:100741. doi:10.1016/j.ymgmr.2021.100741
892 Alqarajeh F, Omorodion J, Bosfield K, Shur N, Ferreira CR. 2020. Lysinuric protein
893 intolerance: Pearls to detect this otherwise easily missed diagnosis. *Transl Sci Rare Dis*
894 **5**:81–86. doi:10.3233/TRD-190035
895 Andriopoulos B, Corradini E, Xia Y, Faasse SA, Chen S, Grgurevic L, Knutson MD,
896 Pietrangelo A, Vukicevic S, Lin HY, Babitt JL. 2009. BMP6 is a key endogenous
897 regulator of hepcidin expression and iron metabolism. *Nat Genet* **41**:482–487.
898 doi:10.1038/ng.335

Barilli A, Rotoli BM, Visigalli R, Bussolati O, Gazzola GC, Gatti R, Dionisi-Vici C, Martinelli D, Goffredo BM, Font-Llitjós M, Mariani F, Luisetti M, Dall'Asta V. 2012. Impaired phagocytosis in macrophages from patients affected by lysinuric protein intolerance. *Mol Genet Metab* **105**:585–589. doi:10.1016/j.ymgme.2012.01.008

Beaumont C, Delaby C. 2009. Recycling Iron in Normal and Pathological States. *Semin Hematol* **46**:328–338. doi:10.1053/j.seminhematol.2009.06.004

Beguin Y. 1998. Prediction of response to optimize outcome of treatment with erythropoietin. *Semin Oncol* **25**:27–34.

Benjamini Y, Hochberg Y. 1995. Controlling the False Discovery Rate: A Practical and Powerful Approach to Multiple Testing. *J R Stat Soc Ser B* **57**:289–300. doi:10.1111/j.2517-6161.1995.tb02031.x

Bennett LF, Liao C, Paulson RF. 2018. Stress erythropoiesis model systemsMethods in Molecular Biology. Humana Press Inc. pp. 91–102. doi:10.1007/978-1-4939-7428-3_5

Bodoy, Sotillo, Espino-Guarch, Sperandeo, Ormazabal, Zorzano, Sebastio, Artuch, Palacín, Bodoy S, Sotillo F, Espino-Guarch M, Sperandeo MP, Ormazabal A, Zorzano A, Sebastio G, Artuch R, Palacín M. 2019. Inducible Slc7a7 Knockout Mouse Model Recapitulates Lysinuric Protein Intolerance Disease. *Int J Mol Sci* **20**:5294. doi:10.3390/ijms20215294

Bolstad B, Collin F, Brettschneider J, Simpson K, Cope L, Irizarry R, Speet T. 2005. Quality Assessment of Affymetrix GeneChip Data In: Gentleman R, Carey V, Huber W, Irizarry R, Dudoit S, editors. Bioinformatics and Computational Biology Solutions Using R and Bioconductor. New York, NY: Springer-Verlag. pp. 33–47. doi:10.1007/0-387-29362-0_3

Bronte V, Zanovello P. 2005. Regulation of immune responses by L-arginine metabolism. *Nat Rev Immunol*. doi:10.1038/nri1668

Chen K, Liu J, Heck S, Chasis JA, An X, Mohandas N. 2009. Resolving the distinct stages in erythroid differentiation based on dynamic changes in membrane protein expression during erythropoiesis. *Proc Natl Acad Sci* **106**:17413–17418. doi:10.1073/pnas.0909296106

Chow A, Huggins M, Ahmed J, Hashimoto D, Lucas D, Kunisaki Y, Pinho S, Leboeuf M, Noizat C, Van Rooijen N, Tanaka M, Zhao ZJ, Bergman A, Merad M, Frenette PS. 2013. CD169 + macrophages provide a niche promoting erythropoiesis under homeostasis and stress. *Nat Med* **19**:429–436. doi:10.1038/nm.3057

Cobbold SA, Llinás M, Kirk K. 2016. Sequestration and metabolism of host cell arginine by the intraerythrocytic malaria parasite *Plasmodium falciparum*. *Cell Microbiol* **18**:820–830. doi:10.1111/cmi.12552

Cohen LA, Gutierrez L, Weiss A, Leichtmann-Bardoogo Y, Zhang DL, Crooks DR, Sougrat R, Morgenstern A, Galy B, Hentze MW, Lazaro FJ, Rouault TA, Meyron-Holtz EG. 2010. Serum ferritin is derived primarily from macrophages through a nonclassical secretory pathway. *Blood* **116**:1574–1584. doi:10.1182/blood-2009-11-253815

Core AB, Canali S, Babitt JL. 2014. Hemojuvelin and bone morphogenetic protein (BMP) signaling in iron homeostasis. *Front Pharmacol*. doi:10.3389/fphar.2014.00104

de Back DZ, Kostova EB, van Kraaij M, van den Berg TK, van Bruggen R. 2014. Of macrophages and red blood cells; a complex love story. *Front Physiol* **5**. doi:10.3389/fphys.2014.00009

Dhanakoti SN, Brosnan JT, Herzberg GR, Brosnan ME. 1990. Renal arginine synthesis: Studies in vitro and in vivo. *Am J Physiol - Endocrinol Metab* **259**. doi:10.1152/ajpendo.1990.259.3.e437

Dichtl S, Haschka D, Nairz M, Seifert M, Volani C, Lutz O, Weiss G. 2018. Dopamine promotes cellular iron accumulation and oxidative stress responses in macrophages. *Biochem Pharmacol* **148**:193–201. doi:10.1016/j.bcp.2017.12.001

Drakesmith H, Nemeth E, Ganz T. 2015. Ironing out Ferroportin. *Cell Metab* **22**:777–787. doi:10.1016/j.cmet.2015.09.006

Durinck S, Spellman PT, Birney E, Huber W. 2009. Mapping identifiers for the integration of genomic datasets with the R/ Bioconductor package biomaRt. *Nat Protoc* **4**:1184–1191.

954 doi:10.1038/nprot.2009.97
955 Efron B, Tibshirani R. 2007. On testing the significance of sets of genes. *Ann Appl Stat*
956 **1**:107–129. doi:10.1214/07-AOAS101
957 Ganz T. 2012. Macrophages and Systemic Iron Homeostasis. *J Innate Immun* **4**:446–453.
958 doi:10.1159/000336423
959 Gautier L, Cope L, Bolstad BM, Irizarry RA. 2004. Affy - Analysis of Affymetrix GeneChip
960 data at the probe level. *Bioinformatics* **20**:307–315. doi:10.1093/bioinformatics/btg405
961 Gentleman RC, Carey VJ, Bates DM, Bolstad B, Dettling M, Dudoit S, Ellis B, Gautier L, Ge
962 Y, Gentry J, Hornik K, Hothorn T, Huber W, Iacus S, Irizarry R, Leisch F, Li C, Maechler
963 M, Rossini AJ, Sawitzki G, Smith C, Smyth G, Tierney L, Yang JYH, Zhang J. 2004.
964 Bioconductor: open software development for computational biology and bioinformatics.
965 *Genome Biol* **5**:R80. doi:10.1186/gb-2004-5-10-r80
966 Goeman JJ, Bühlmann P. 2007. Analyzing gene expression data in terms of gene sets:
967 Methodological issues. *Bioinformatics* **23**:980–987. doi:10.1093/bioinformatics/btm051
968 Goldfarb AN, Freeman KC, Sahu RK, Elagib KE, Holy M, Arneja A, Polanowska-Grabowska
969 R, Gru AA, White Z, Khalil S, Kerins MJ, Ooi A, Leitinger N, Luckey CJ, Delehanty LL.
970 2021. Iron control of erythroid microtubule cytoskeleton as a potential target in
971 treatment of iron-restricted anemia. *Nat Commun* **12**. doi:10.1038/s41467-021-21938-2
972 Gonzalez-Roca E, Garcia-Albéniz X, Rodriguez-Mulero S, Gomis RR, Kornacker K, Auer H.
973 2010. Accurate Expression Profiling of Very Small Cell Populations. *PLoS One*
974 **5**:e14418. doi:10.1371/journal.pone.0014418
975 Guo M, Härtlova A, Gierliński M, Prescott A, Castellvi J, Losa JH, Petersen SK, Wenzel UA,
976 Dill BD, Emmerich CH, Ramon Y Cajal S, Russell DG, Trost M. 2019. Triggering MSR1
977 promotes JNK-mediated inflammation in IL-4-activated macrophages. *EMBO J* **38**:1–
978 15. doi:10.15252/embj.2018100299
979 Haldar M, Kohyama M, So AY-L, KC W, Wu X, Briseño CG, Satpathy AT, Kretzer NM, Arase
980 H, Rajasekaran NS, Wang L, Egawa T, Igarashi K, Baltimore D, Murphy TL, Murphy
981 KM. 2014. Heme-Mediated SPI-C Induction Promotes Monocyte Differentiation into
982 Iron-Recycling Macrophages. *Cell* **156**:1223–1234. doi:10.1016/j.cell.2014.01.069
983 Hattangadi SM, Wong P, Zhang L, Flygare J, Lodish HF. 2011. From stem cell to red cell:
984 regulation of erythropoiesis at multiple levels by multiple proteins, RNAs, and chromatin
985 modifications. *Blood* **118**:6258–6268. doi:10.1182/blood-2011-07-356006
986 Hussell T, Bell TJ. 2014. Alveolar macrophages: plasticity in a tissue-specific context. *Nat*
987 *Rev Immunol* **14**:81–93. doi:10.1038/nri3600
988 Irizarry RA. 2003. Exploration, normalization, and summaries of high density oligonucleotide
989 array probe level data. *Biostatistics* **4**:249–264. doi:10.1093/biostatistics/4.2.249
990 Jd T, Th B. 1968. A simple technique for measuring storage iron concentrations in
991 formalinised liver samples. *S Afr J Med Sci* **33**:9–11.
992 Jelkmann W. 2011. Regulation of erythropoietin production. *J Physiol* **589**:1251–1258.
993 doi:10.1113/jphysiol.2010.195057
994 Jha AK, Huang SC-CC, Sergushichev A, Lampropoulou V, Ivanova Y, Loginicheva E,
995 Chmielewski K, Stewart KM, Ashall J, Everts B, Pearce EJ, Driggers EM, Artyomov MN.
996 2015. Network integration of parallel metabolic and transcriptional data reveals
997 metabolic modules that regulate macrophage polarization. *Immunity* **42**:419–430.
998 doi:10.1016/j.immuni.2015.02.005
999 JL B, FW H, DM W, Y X, Y S, TA S, JA C, RT C, AL S, CJ W, NC A, HY L. 2006. Bone
1000 morphogenetic protein signaling by hemojuvelin regulates hepcidin expression. *Nat*
1001 *Genet* **38**:531–539. doi:10.1038/NG1777
1002 Kawasumi H, Gono T, Kawaguchi Y, Kaneko H, Katsumata Y, Hanaoka M, Kataoka S,
1003 Yamanaka H. 2014. IL-6, IL-8, and IL-10 are associated with hyperferritinemia in rapidly
1004 progressive interstitial lung disease with polymyositis/dermatomyositis. *Biomed Res Int*
1005 **2014**. doi:10.1155/2014/815245
1006 Klei TRL, Meinderts SM, van den Berg TK, van Bruggen R. 2017. From the Cradle to the
1007 Grave: The Role of Macrophages in Erythropoiesis and Erythrophagocytosis. *Front*
1008 *Immunol* **8**:73. doi:10.3389/fimmu.2017.00073

Knutson MD, Oukka M, Koss LM, Aydemir F, Wessling-Resnick M. 2005. Iron release from macrophages after erythrophagocytosis is up-regulated by ferroportin 1 overexpression and down-regulated by hepcidin. *Proc Natl Acad Sci* **102**:1324–1328. doi:10.1073/pnas.0409409102

Koh TJ, DiPietro LA. 2011. Inflammation and wound healing: the role of the macrophage. *Expert Rev Mol Med*. doi:10.1017/S1462399411001943

Kohyama M, Ise W, Edelson BT, Wilker PR, Hildner K, Mejia C, Frazier WA, Murphy TL, Murphy KM. 2009. Role for Spi-C in the development of red pulp macrophages and splenic iron homeostasis. *Nature* **457**:318–321. doi:10.1038/nature07472

Kuhn V, Diederich L, Keller TCS, Kramer CM, Lückstädt W, Panknin C, Suvorava T, Isakson BE, Kelm M, Cortese-Krott MM. 2017. Red Blood Cell Function and Dysfunction: Redox Regulation, Nitric Oxide Metabolism, Anemia. *Antioxid Redox Signal* **26**:718–742. doi:10.1089/ars.2016.6954

Lee JCM, Gimm JA, Lo AJ, Koury MJ, Krauss SW, Mohandas N, Chasis JA. 2004. Mechanism of protein sorting during erythroblast enucleation: Role of cytoskeletal connectivity. *Blood* **103**:1912–1919. doi:10.1182/blood-2003-03-0928

Liberzon A, Birger C, Thorvaldsdóttir H, Ghandi M, Mesirov JP, Tamayo P. 2015. The Molecular Signatures Database Hallmark Gene Set Collection. *Cell Syst* **1**:417–425. doi:10.1016/j.cels.2015.12.004

Liu S, McConnell SC, Ryan TM. 2013. Erythropoiesis in the Absence of Adult Hemoglobin. *Mol Cell Biol* **33**:2241–2251. doi:10.1128/mcb.01734-12

Lukkarinen M, Näntö-Salonen K, Pulkki K, Aalto M, Simell O. 2003. Oral supplementation corrects plasma lysine concentrations in lysinuric protein intolerance. *Metabolism* **52**:935–938. doi:10.1016/S0026-0495(03)00089-1

Luo B, Gan W, Liu Z, Shen Z, Wang J, Shi R, Liu Yuqi, Liu Yu, Jiang M, Zhang Z, Wu Y. 2016. Erythropoeitin Signaling in Macrophages Promotes Dying Cell Clearance and Immune Tolerance. *Immunity* **44**:287–302. doi:10.1016/j.immuni.2016.01.002

Mauhin W, Habarou F, Gobin S, Servais A, Brassier A, Grisel C, Roda C, Pinto G, Moshous D, Ghalim F, Krug P, Deltour N, Pontoizeau C, Dubois S, Assoun M, Galmiche L, Bonnefont J, Ottolenghi C, de Blic J, Arnoux J, de Lonlay P. 2017. Update on Lysinuric Protein Intolerance, a Multi-faceted Disease Retrospective cohort analysis from birth to adulthood. *Orphanet J Rare Dis* **12**:3. doi:10.1186/s13023-016-0550-8

Moestrup S, Møller H. 2004. CD163: a regulated hemoglobin scavenger receptor with a role in the anti-inflammatory response. *Ann Med* **36**:347–354. doi:10.1080/07853890410033171

Moritz KM, Lim GB, Wintour EM. 1997. Developmental regulation of erythropoietin and erythropoiesis. *Am J Physiol Integr Comp Physiol* **273**:R1829–R1844. doi:10.1152/ajpregu.1997.273.6.R1829

Morris SM. 2002. REGULATION OF ENZYMES OF THE UREA CYCLE AND ARGININE METABOLISM. doi:10.1146/annurev.nutr.22.110801.140547

Murray PJ, Wynn TA. 2011. Protective and pathogenic functions of macrophage subsets. *Nat Rev Immunol* **11**:723–737. doi:10.1038/nri3073

Nairz M, Schleicher U, Schroll A, Sonnweber T, Theurl I, Ludwiczek S, Talasz H, Brandacher G, Moser PL, Muckenthaler MU, Fang FC, Bogdan C, Weiss G. 2013. Nitric oxide–mediated regulation of ferroportin-1 controls macrophage iron homeostasis and immune function in Salmonella infection. *J Exp Med* **210**:855–873. doi:10.1084/jem.20121946

Nemeth E, Ganz T. 2009. The Role of Hepcidin in Iron Metabolism. *Acta Haematol* **122**:78–86. doi:10.1159/000243791

Nemeth E, Tuttle MS, Powelson J, Vaughn MB, Donovan A, Ward DM, Ganz T, Kaplan J. 2004. Hepcidin regulates cellular iron efflux by binding to ferroportin and inducing its internalization. *Science* **306**:2090–3. doi:10.1126/science.1104742

Oexle H, Kaser A, Möst J, Bellmann-Weiler R, Werner ER, Werner-Felmayer G, Weiss G. 2003. Pathways for the regulation of interferon-γ-inducible genes by iron in human monocytic cells. *J Leukoc Biol* **74**:287–294. doi:10.1189/jlb.0802420

Ogier de Baulny H, Schiff M, Dionisi-Vici C. 2012. Lysinuric protein intolerance (LPI): a multi organ disease by far more complex than a classic urea cycle disorder. *Mol Genet Metab* **106**:12–7. doi:10.1016/j.ymgme.2012.02.010

Oldenborg P-A. 2000. Role of CD47 as a Marker of Self on Red Blood Cells. *Science (80-)* **288**:2051–2054. doi:10.1126/science.288.5473.2051

Palacín M, Borsani G, Sebastio G. 2001. The molecular bases of cystinuria and lysinuric protein intolerance. *Curr Opin Genet Dev* **11**:328–335. doi:10.1016/S0959-437X(00)00198-2

Palacín M, Nunes V, Font-Llitjós M, Jiménez-Vidal M, Fort J, Gasol E, Pineda M, Feliubadaló L, Chillarón J, Zorzano A. 2005. The Genetics of Heteromeric Amino Acid Transporters. *Physiology* **20**:112–124. doi:10.1152/physiol.00051.2004

Park SY, Kim IS. 2017. Engulfment signals and the phagocytic machinery for apoptotic cell clearance. *Exp Mol Med*. doi:10.1038/emm.2017.52

Parto K, Maki J, Pelliniemi LJ, Simell O. 1994. Abnormal pulmonary macrophages in lysinuric protein intolerance: Ultrastructural, morphometric, and x-ray microanalytic study. *Arch Pathol Lab Med* **118**:536–541.

Patel BN, Dunn RJ, Jeong SY, Zhu Q, Julien JP, David S. 2002. Ceruloplasmin regulates iron levels in the CNS and prevents free radical injury. *J Neurosci* **22**:6578–6586. doi:10.1523/jneurosci.22-15-06578.2002

Perkins CP, Mar V, Shutter JR, Castillo J Del, Danilenko DM, Medlock ES, Ponting IL, Graham M, Stark KL, Zuo Y, Cunningham JM, Bosselman RA. 1997. Anemia and perinatal death result from loss of the murine ecotropic retrovirus receptor mCAT-1. *Genes Dev* **11**:914–925. doi:10.1101/gad.11.7.914

Pollard JW. 2009. Trophic macrophages in development and disease. *Nat Rev Immunol* **9**:259–270. doi:10.1038/nri2528

Popova EY, Krauss SW, Short SA, Lee G, Villalobos J, Etzell J, Koury MJ, Ney PA, Chasis JA, Grigoryev SA. 2009. Chromatin condensation in terminally differentiating mouse erythroblasts does not involve special architectural proteins but depends on histone deacetylation. *Chromosom Res* **17**:47–64. doi:10.1007/s10577-008-9005-y

Posey JE, Burrage LC, Miller MJ, Liu P, Hardison MT, Elsea SH, Sun Q, Yang Y, Willis AS, Schlesinger AE, Bacino CA, Lee BH. 2014. Lysinuric protein intolerance presenting with multiple fractures. *Mol Genet Metab Reports* **1**:176–183. doi:10.1016/j.ymgmr.2014.03.004

R Core T. 2019. R: A language and environment for statistical computing. R Foundation for Statistical Computing. *Vienna, Austria*. https://www.r-project.org/.

Rajantie J, Simell O, Rapola J, Perheentupa J. 1980. Lysinuric protein intolerance: A two-year trial of dietary supplementation therapy with citrulline and lysine. *J Pediatr* **97**:927–932. doi:10.1016/S0022-3476(80)80422-7

Recalcati S, Locati M, Gammella E, Invernizzi P, Cairo G. 2012. Iron levels in polarized macrophages: Regulation of immunity and autoimmunity. *Autoimmun Rev*. doi:10.1016/j.autrev.2012.03.003

Ritchie ME, Phipson B, Wu D, Hu Y, Law CW, Shi W, Smyth GK. 2015. Limma powers differential expression analyses for RNA-sequencing and microarray studies. *Nucleic Acids Res* **43**:e47. doi:10.1093/nar/gkv007

Rosário C, Zandman-Goddard G, Meyron-Holtz EG, D'Cruz DP, Shoenfeld Y. 2013. The Hyperferritinemic Syndrome: macrophage activation syndrome, Still's disease, septic shock and catastrophic antiphospholipid syndrome. *BMC Med* **11**:185. doi:10.1186/1741-7015-11-185

Rotoli BM, Barilli A, Visigalli R, Ferrari F, Dall'Asta V. 2020. y+LAT1 and y+LAT2 contribution to arginine uptake in different human cell models: Implications in the pathophysiology of Lysinuric Protein Intolerance. *J Cell Mol Med* **24**:921–929. doi:10.1111/jcmm.14801

Sebastiani G, Wilkinson N, Pantopoulos K. 2016. Pharmacological targeting of the hepcidin/ferroportin axis. *Front Pharmacol* **7**:1–11. doi:10.3389/fphar.2016.00160

Shima Y, Maeda T, Aizawa S, Tsuboi I, Kobayashi D, Kato R, Tamai I. 2006. HEMATOPOIESIS L -arginine import via cationic amino acid transporter CAT1 is

essential for both differentiation and proliferation of erythrocytes. *Blood* **107**:1352–1356. doi:10.1182/blood-2005-08-3166.Reprints

Smyth GK. 2004. Linear models and empirical bayes methods for assessing differential expression in microarray experiments. *Stat Appl Genet Mol Biol* **3**. doi:10.2202/1544-6115.1027

Soares MP, Hamza I. 2016. Macrophages and Iron Metabolism. *Immunity*. doi:10.1016/j.immuni.2016.02.016

Stienstra R, Netea-Maier RT, Riksen NP, Joosten LAB, Netea MG. 2017. Specific and Complex Reprogramming of Cellular Metabolism in Myeloid Cells during Innate Immune Responses. *Cell Metab*. doi:10.1016/j.cmet.2017.06.001

Swartz KL, Wood SN, Murthy T, Ramirez O, Qin G, Pillai MM, Rao S, Minella AC. 2017. E2F-2 Promotes Nuclear Condensation and Enucleation of Terminally Differentiated Erythroblasts. *Mol Cell Biol* **37**. doi:10.1128/mcb.00274-16

Theurl I, Hilgendorf I, Nairz M, Tymoszuk P, Haschka D, Asshoff M, He S, Gerhardt LMS, Holderried TAW, Seifert M, Sopper S, Fenn AM, Anzai A, Rattik S, McAlpine C, Theurl M, Wieghofer P, Iwamoto Y, Weber GF, Harder NK, Chousterman BG, Arvedson TL, McKee M, Wang F, Lutz OMD, Rezoagli E, Babitt JL, Berra L, Prinz M, Nahrendorf M, Weiss G, Weissleder R, Lin HY, Swirski FK. 2016. On-demand erythrocyte disposal and iron recycling requires transient macrophages in the liver. *Nat Med* **22**:945–951. doi:10.1038/nm.4146

Torrents D, Mykkänen J, Pineda M, Feliubadaló L, Estévez R, de Cid R, Sanjurjo P, Zorzano A, Nunes V, Huoponen K, Reinikainen A, Simell O, Savontaus M-LL, Aula P, Palacín M, Cid Rafael de, Sanjurjo P, Zorzano A, Nunes V, Huoponen K, Reinikainen A, Simell O, Savontaus M-LL, Aula P, Palacín M, de Cid R, Sanjurjo P, Zorzano A, Nunes V, Huoponen K, Reinikainen A, Simell O, Savontaus M-LL, Aula P, Palacín M. 1999. Identification of SLC7A7, encoding y+LAT-1, as the lysinuric protein intolerance gene. *Nat Genet* **21**:293–296. doi:10.1038/6809

Weiss G, Schaible UE. 2015. Macrophage defense mechanisms against intracellular bacteria. *Immunol Rev* **264**:182–203. doi:10.1111/imr.12266

Wu D, Lim E, Vaillant F, Asselin-Labat ML, Visvader JE, Smyth GK. 2010. ROAST: Rotation gene set tests for complex microarray experiments. *Bioinformatics* **26**:2176–2182. doi:10.1093/bioinformatics/btq401